

**ASSISTED METHANE HYDRATE FORMATION WITH THE ADDITION  
OF PROMOTERS**

Chutikan Jaikwang

A Thesis Submitted in Partial Fulfillment of the Requirements  
for the Degree of Master of Science  
The Petroleum and Petrochemical College, Chulalongkorn University  
in Academic Partnership with  
The University of Michigan, The University of Oklahoma,  
Case Western Reserve University, and Institut Français du Pétrole  
2017

บทคัดย่อและแฟ้มข้อมูลฉบับเต็มของวิทยานิพนธ์ตั้งแต่ปีการศึกษา 2554 ที่ให้บริการในคลังปัญญาจุฬาฯ (CUIR)  
เป็นแฟ้มข้อมูลของนิสิตเจ้าของวิทยานิพนธ์ที่ส่งผ่านทางบัณฑิตวิทยาลัย

The abstract and full text of theses from the academic year 2011 in Chulalongkorn University Intellectual Repository (CUIR)  
are the thesis authors' files submitted through the Graduate School.

**Thesis Title:** Assisted Methane Hydrate Formation with the Addition of Promoters  
**By:** Chutikan Jaikwang  
**Program:** Petrochemical Technology  
**Thesis Advisors:** Prof. Pramoch Rangsunvigit  
Dr. Santi Kulprathipanja

---

Accepted by The Petroleum and Petrochemical College, Chulalongkorn University, in partial fulfilment of the requirements for the Degree of Master of Science.

..... College Dean  
(Prof. Suwabun Chirachanchai)

**Thesis Committee:**

.....  
(Prof. Pramoch Rangsunvigit)

.....  
(Dr. Santi Kulprathipanja)

.....  
(Assoc. Prof. Boonyarach Kitiyanan)

.....  
(Dr. Tanate Danuthai)

## ABSTRACT

5871002063: Petrochemical Technology Program

Chutikan Jaikwang: Assisted Methane Hydrate Formation with the Addition of Promoters

Thesis Advisors: Prof. Pramoch Rangsunvigit and Dr. Santi Kulprathipanja 63 pp.

Keywords: Methane hydrate/TBAB/ Cyclopentane/Hydrate formation

Natural gas hydrates play an important role in the largest reservoir of hydrocarbons on earth. The gas hydrates have received increasing attention in an excellent way of new technology for gas in large quantity storage and transportation. However, the main challenge to use methane hydrates has faced many challenges such as the slow formation rate, low growth rate during hydrate formation, and low conversion ratio of gas to solid hydrates leading to poor storage capacity. In this work, methane hydrate formation and dissociation in the presence of different Cyclopentane (CP), Tetra-n-butyl phosphonium bromide (TBPB) and Tetra-n-butyl ammonium bromide (TBAB) concentrations were investigated. The formation experiment was conducted in an unstirred system. The temperature was controlled between 2.5 and 4.0°C at 8 MPa. The hydrate dissociation experiment was performed after the completion of hydrate formation. The results showed that the presence of TBPB alone was not sufficient to promote methane hydrate formation. The addition of TBAB promoted methane hydrate formation with only small amount of methane uptake. Increasing the concentration of CP improved methane consumption. However, the methane consumption in the presence of CP was higher than that with TBAB.

## บทคัดย่อ

ชุติกายุจน์ ใจกว้าง: การศึกษาการเกิดและการสลายตัวของมีเทนไฮเดรตโดยใช้สารส่งเสริม (Assisted Methane Hydrate Formation with the Addition of Promoters) อ. ที่ปรึกษา : ศ. ดร. ปราโมช รังสรรค์วิจิตร และ ดร. สันติ กุลประทีปปัญญา 63 หน้า

แก๊สไฮเดรตเป็นพลังงานทางเลือกที่สำคัญและมีบทบาทในการกักเก็บและการขนส่งแก๊สธรรมชาติในรูปแบบใหม่ อย่างไรก็ตามกระบวนการเกิดแก๊สไฮเดรตนั้นใช้เวลานานและความดันสูงซึ่งเป็นอุปสรรคในเชิงอุตสาหกรรมการกักเก็บและการขนส่ง เตตระบิวทิลฟอสโฟรเนียมโบรไมด์ (TBPB), เตตระบิวทิลแอมโมเนียมโบรไมด์ (TBAB) และ โซโคลเพนเทน (CP) เป็นตัวเร่งชนิดอุณหภูมิศาสตร์ซึ่งสามารถเกิดโครงสร้างไฮเดรตที่สภาวะความดันบรรยากาศและอุณหภูมิเหนือศูนย์องศาเซลเซียส ในการศึกษาครั้งนี้ได้ทำการทดลองและศึกษาอิทธิพลของสารละลาย เตตระบิวทิลฟอสโฟรเนียมโบรไมด์ (TBPB), เตตระบิวทิลแอมโมเนียมโบรไมด์ (TBAB) และ โซโคลเพนเทน (CP) ต่อกลไกการเกิดและการสลายตัวของมีเทนไฮเดรต ในสภาวะที่ไม่มีการรบกวนที่อุณหภูมิคงที่และทำการเปรียบเทียบกับระบบน้ำบริสุทธิ์ โดยใช้สารละลายที่ความเข้มข้นต่างๆโดยดำเนินการในระบบปิดที่ 8 เมกะปาสคาล อุณหภูมิ 2.5 และ 4 องศาเซลเซียส กระบวนการสลายตัวของมีเทนไฮเดรตดำเนินการภายหลังจากกระบวนการเกิดมีเทนไฮเดรตเสร็จสมบูรณ์ ผลการทดลองสรุปได้ว่า เตตระบิวทิลฟอสโฟรเนียมโบรไมด์ (TBPB) ไม่สามารถส่งเสริมการเกิดมีเทนไฮเดรต และเตตระบิวทิลแอมโมเนียมโบรไมด์ (TBAB) ช่วยส่งเสริมการเกิดมีเทนไฮเดรตแต่กักเก็บก๊าซได้ปริมาณน้อย ในขณะที่โซโคลเพนเทน (CP) ช่วยส่งเสริมการเกิดมีเทนไฮเดรต การเพิ่มปริมาณโซโคลเพนเทนทำให้ใช้เวลาในการเกิดมีเทนไฮเดรตเพิ่มขึ้นและเพิ่มปริมาณการกักเก็บแก๊สมีเทนเมื่อเปรียบเทียบกับระบบน้ำบริสุทธิ์

## ACKNOWLEDGEMENTS

I would like to express my sincere gratitude to my advisor, Prof. Pramoch Rangsunvigit, for his beneficial recommendations, and supervision from the very early stage of my research. He also provided me unflinching encouragement, patience, and all supports throughout my graduate research.

I also would like to thank my co-advisors, Dr. Santi Kulprathipanja, for his advices, guidance, and willingness to share his knowledge and experience with me, which was very helpful for research inspiration.

I would like to thank to the thesis committees, Assoc. Prof. Boonyarach Kitiyanan and Dr. Tanate Danuthai for their important suggestions and beneficial recommendations in my research.

I am grateful for the full scholarship and full funding of the thesis work provided by the Petroleum and Petrochemical College.

I am grateful for the scholarship and funding of the thesis work provided by the Petroleum and Petrochemical College and The 90<sup>th</sup> Anniversary of Chulalongkorn University Fund and Grant for International Integration: Chula Research Scholar, Ratchadaphiseksomphot Endowment Fund, Chulalongkorn University, Thailand; The Petroleum and Petrochemical College and the Center of Excellence for Petrochemical and Materials Technology, Thailand.

I would like to thank the entire faculty and staff at The Petroleum and Petrochemical College, Chulalongkorn University for their kind assistance and cooperation.

I would like to thank Mr. Atsawuth Siangsai, Mr. Katipot Inkong, Mr. Soravis Limvisitsakul and Ms. Warintip Chanakro for their suggestion and help.

Finally, I would like to express my sincere gratitude to my family for supporting intellectual pursuit ever since I was a child and help me grow in many ways, for staying by me and for understanding every part of my mind.

## TABLE OF CONTENTS

	<b>PAGE</b>
Title Page	i
Abstract (in English)	iii
Abstract (in Thai)	iv
Acknowledgements	v
Table of Contents	vi
List of Tables	viii
List of Figures	ix
 <b>CHAPTER</b>	
<b>I INTRODUCTION</b>	<b>1</b>
 <b>II THEORETICAL BACKGROUND AND LITERATURE REVIEW</b>	 <b>3</b>
2.1 Methane Hydrate	3
2.2 Gas Hydrates Properties	7
2.3 Methane Hydrates in Natural Resources	9
2.4 Gas Hydrate Formation	10
2.5 Methane Hydrate Stability	11
2.6 Gas Hydrate Dissociation	13
2.7 Physical Chemistry of Methane Hydrates	14
2.7.1 Thermodynamics	14
2.7.2 Kinetics	14
2.8 Natural Gas Hydrate Transportation	15
2.9 Promotion of Gas Hydrate Formation	16

<b>CHAPTER</b>	<b>PAGE</b>	
<b>III</b>	<b>EXPERIMENTAL</b>	30
	3.1 Materials and Equipment	30
	3.1.1 Materials	30
	3.1.2 Equipment	30
	3.2 Experimental Procedures	30
	3.2.1 Experimental Apparatus	30
	3.2.2 Methane Hydrate Formation	32
	3.2.3 Methane Hydrate Dissociation	33
<b>IV</b>	<b>RESULTS AND DISCUSSION</b>	35
	4.1 Effects of Tetrabutylphosphonium bromide (TBPB)	35
	4.2 Effects of Tetra-n-butyl ammonium bromide (TBAB)	36
	4.3 Effects of Cyclopentane (CP)	38
	4.3.1 Methane Hydrate Formation	38
	4.3.2 Effects of Experimental Temperature	44
	4.3.3 Methane Hydrate Dissociation	47
<b>V</b>	<b>CONCLUSIONS AND RECOMMENDATIONS</b>	52
	5.1 Conclusions	52
	5.2 Recommendations	52
	<b>REFERENCES</b>	53
	<b>APPENDICES</b>	58
	<b>Appendix A</b> Calculation for the Methane Consumption	58
	<b>Appendix B</b> Calculation for the Methane Hydrate Yield	61
	<b>Appendix B</b> Calculation for the Percentage of Methane Recovery	61
	<b>CURRICULUM VITAE</b>	63

## LIST OF TABLES

TABLE		PAGE
2.1	Properties of different hydrate structures	5
2.2	Comparison of properties of ice, sI, and sII hydrate crystal structures	7
4.1	Experimental conditions for methane hydrate formation with TBAB at 2.5°C and 8 MPa	37
4.2	Experimental conditions for methane hydrate formation with CP at 2.5°C and 8 MPa	39
4.3	Experimental conditions for methane hydrate formation with 10% V/V of CP at 2.5°C and 4°C (8MPa)	45
4.4	Experimental conditions for methane hydrate dissociation in presence of CP at various % V/V	48
4.5	Methane released and methane recovery in presence of CP at various % V/V.	49
4.6	Experimental conditions for methane hydrate formation with 15% V/V of CP at 2.5°C and 4°C (8MPa)	50



## LIST OF FIGURES

FIGURE		PAGE
2.1	Model of a methane molecule enclosed in water-molecule “cage”	3
2.2	Progress of research activity on “natural gas hydrates” or “methane hydrates”	4
2.3	Methane hydrate dissociation with the methane ignited	5
2.4	Three most common hydrate structures, sI, sII, sH, and the number of cages, which make up their respective unit cells	6
2.5	Location of sampled and inferred gas	9
2.6	Hydrate growth from nucleation for the mixed hydrogen/propane hydrate formation experiment conducted with water	11
2.7	Phase boundary diagram demonstrating the gas hydrate stability field in gray	12
2.8	Schematic of gas recovery from gas hydrate methods	13
2.9	Hydrate transportation chain	15
2.10	Structure of TBPB	17
2.11	Structure of TBAB	17
2.12	Structure of CP	17
2.13	The evolutions of the methane consumption during the hydrate growth period (the initial pressure was 6 MPa, the temperature was 275.15 K and the water was 1.67 mol)	18
2.14	The gas hydrate induction time variations with the initial pressure	19
2.15	Maximum dissociated methane as mole percent for different maize starch concentrations at temperatures minus 4 °C and minus 1 °C	20
2.16	Unit cell of the presently found TBPB hydrate crystal. Atom types are denoted as follows: green: carbon; red: oxygen; pink: phosphorus; yellow: bromine. Hydrogen atoms are omitted for clarity	21
2.17	Hydrate crystal growth and oligo crystals of TBPB at $w_{\text{TBPB}} = 0.35$ and $T_{\text{ex}} = 281.2$ K	22

<b>FIGURE</b>	<b>PAGE</b>
2.18 25 wt% TBPB hydrate formation of semihydrates with different additives	24
2.19 Hydrate dissociation for CH <sub>4</sub> + TBAB+ water	24
2.20 Sequential photos of the growth of TBPB semihydrates crystals at $w = 0.10$ , $\Delta T_{\text{sub}} = 4.7$ K at atmospheric pressure	26
2. 21 Formation temperature of single/binary TBAF hydrate	26
2.22 Equilibrium $P$ versus $T$ condition for three phase involving hydrate in tetrabutylphosphonium bromide(TBPB)-containing systems: $\circ$ , O <sub>2</sub> + TBPB + water system; $\blacktriangle$ , CO <sub>2</sub> + TBPB + water system; $\square$ , CH <sub>4</sub> + TBPB + water system; $\diamond$ , N <sub>2</sub> + TBPB + water system. The mass fraction or mole fraction of TBPB in the solution $w_{\text{TBPB}} = 0.35$	27
2.23 Pictorial illustration of the mechanism of CO <sub>2</sub> -H <sub>2</sub> -CP hydrates in an unstirred system.	28
2.24 Gas uptake change for hydrate formation vs. time from different systems at 276.15 K and 4.0 MPa	29
3.1 Schematic of the experimental apparatus.	31
3.2 Cross-section of a crystallizer.	32
4.1 Gas uptake and temperature profiles of forming TBAB hydrate at 2.5°C and 8 MPa in batch operation (in the presence of 2.56 mol% TBPB).	35
4.2 Gas uptake and temperature profiles of forming TBAB hydrate at 2.5°C and 8 MPa in batch operation (in the presence of 2.56 mol% TBAB) (experiment 2).	37
4.3 Effects of CP concentrations (% V/V) on induction time.	38
4.4 Effects of CP concentrations (% V/V) on methane consumed.	40
4.5 Typical methane consumption and temperature profiles during the methane hydrate formation experiments performed with 10% V/V at 2.5°C (Experiment 7, Table 4.2).	41

<b>FIGURE</b>	<b>PAGE</b>
4.6 Pictorial illustration of the mechanism of CO <sub>2</sub> -H <sub>2</sub> -CP hydrates in an unstirred system	42
4.7 Typical methane consumption and temperature profiles during the methane hydrate formation experiments performed with CP at 2.5°C: (a) 10% V/V (Experiment 7, Table 4.2), (b) 15% V/V (Experiment 11, Table 4.2)	43
4.8 Effects of CP concentrations (% V/V) on methane hydrate yield.	44
4.9 Typical methane consumption and temperature profiles during the methane hydrate formation experiments performed with CP at 8 Mpa : (a) 15% V/V CP at 4°C, (b) 15% V/V (Experiment 11, Table 4.2).	46
4.10 Typical methane released and temperature profiles during methane hydrate dissociation with the presence of 15% V/V of CP (Experiment 10, Table 4.3).	47
4.11 Typical methane released and temperature profiles during methane hydrate dissociation with the presence of 10% V/V CP: (a) 2.5°C (Experiment 8, Table 4.6), (b) 4°C (Experiment 16, Table 4.6).	51

## **CHAPTER I**

### **INTRODUCTION**

In recent years, the global energy demands have been continually increased due to the growth of human society. More than 76% of energy will come from carbon based source such as gas, oil, and coal. Among these three carbons based energy sources, natural gas is present to the highest rate as compared to the other sources of fossil energy ([www.corporate.exxonmobil.com](http://www.corporate.exxonmobil.com)).

Natural gas hydrates play an important role in the largest reservoir of hydrocarbons in the earth and a possible energy resource for the coming age due to clean energy sources. The gas hydrates have received increasing attention in an excellent way of new technology for gas in large quantity storage and transportation. The transportation cost of natural gas hydrates is expected to be 18-24% lower than the liquefied natural gas (LNG) (Gudmundsson *et al.*, 2002).

Natural gas hydrates consist of methane gas, the molecule of which is trapped in the hydrogen-bonded water cages under the high pressure and low temperature. A volume of methane hydrates contains 164 times volume of natural gas at standard conditions (STP) (Sloan, 1998a). However, the main challenge to use methane hydrates in industrial processes has faced many challenges such as the slow formation rate, low growth rate during hydrate formation, and low conversion ratio of gas to solid hydrates leading to poor storage capacity. Therefore, scientific methods that can increase the formation rate as well as gas uptake have been studied (Zarenezhad and Varaminian, 2013). Hydrate promoters are one of alternative choices that may overcome these problems. Gas hydrate promoters can be divided to two types. One is thermodynamic promoters, which can assist the hydrate formation conditions to low pressure and high temperature. The other one is kinetic promoters, which increase the rate of hydrate formation (Sloan, 1998a).

Several studies have reported that the kinetics promoters such as sodium dodecyl sulfate (SDS) and sodium dodecyl benzene sulfonate (SDBS) had positive influence on the hydrate formation rates (Li *et al.*, 2012a). However, the thermodynamic promoters such as tetra-n-butyl ammonium bromide (TBAB) and

tetrahydrofuran (THF) took part in the hydrate formation and significantly reduced the gas hydrates and formation pressures (Cai *et al.*, 2016).

Tetrabutylphosphonium bromide (TBPB), tetra-n-butyl ammonium bromide (TBAB), and cyclopentane (CP) are thermodynamic promoters. Many works have been sought to find TBPB, TBAB, and CP mixing ratios that give optimal hydrate phase equilibrium.

Muromachi *et al.* (2014) found that the stoichiometric composition for TBPB hydrates is  $\text{TBPB} \cdot 32\text{H}_2\text{O}$ . The structure features three dodecahedral cages for each TBPB molecule may accommodate small gas molecules like  $\text{CH}_4$ ,  $\text{CO}_2$ , and  $\text{N}_2$ . Sun and Sun (2010) studied phase equilibrium of semiclathrate for TBAB + methane (mass fraction range of 0.05 to 0.45) and found that TBAB can reduce the formation pressure of gas hydrate. Duc *et al.* (2007) presented the thermodynamic data showing that the addition of 0.29 mol% TBAB can substantially decrease the formation pressure of the  $\text{CO}_2/\text{N}_2$  hydrates. Lim *et al.* (2013) investigated the morphology of  $\text{CO}_2/\text{H}_2/\text{CP}$  mixed hydrates in an unstirred system and presented the mechanism of hydrate formation in quiescent conditions. They proposed that, at the CP–water interface, hydrates begin to grow upward and radially inward towards the center of the reactor. Li *et al.* (2012b) investigated the synergic effect of CP and TBAB on the  $\text{CO}_2$  hydrate. They found that the CP molecules housed in the large cavities together with TBAB cations ( $\text{TBA}^+$ ) make the semi-hydrate more stable resulting in increase of the gas uptake.

This work will focus on the formation of methane hydrates using tetrabutylphosphonium bromide (TBPB), tetra-n-butyl ammonium bromide (TBAB) and cyclopentane (CP) as promoters in terms of kinetic and thermodynamic point of view compared with the pure water system. In addition, the effects of the promoters on the methane hydrate dissociation will be observed.

## CHAPTER II

### THEORETICAL BACKGROUND AND LITERATURE REVIEW

#### 2.1 Methane Hydrates

Methane hydrates, also called methane clathrate or gas hydrates, are like solid lattice that consists of a gas molecule surrounded by a cage of water molecules. It is similar to ice, except that the crystalline structure composes the guest gas molecule within the cage of water molecules. The model of a methane molecule enclosed in water-molecule or is shown in Figure 2.1 ([www.minerals.usgs.gov](http://www.minerals.usgs.gov)).

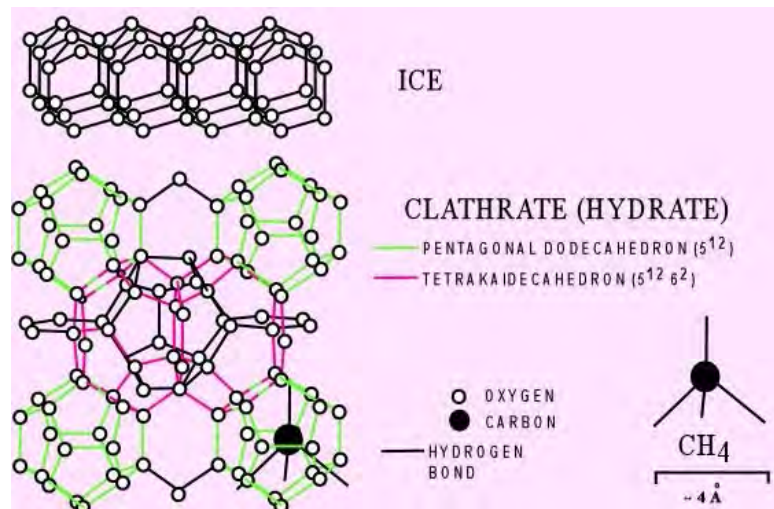


**Figure 2.1** Model of a methane molecule enclosed in water-molecule “cage” ([www7430.nrlssc.navy.mil](http://www7430.nrlssc.navy.mil)).

Methane hydrates are widespread in sea sediments more than hundreds of meters below the sea floor, along the outer continental margins. They are also found in Arctic permafrost. Some of hydrates are deposited close to the ocean floor and at water depths as shallow as 150 m. At low latitudes, the methane hydrates are generally only found below 500 m. The hydrates can be deposited around 300–600 m thick in cover large horizontal areas. The average hydrates composition is 1 mole of methane for every 5.75 mole of water. The density of the hydrates is around

0.9 kg/L. One liter of methane hydrates solid would contain 168 L of methane gas at STP (Demirbas, 2010).

In recent years, hydrate formation is found to be a major problem, clogging pipelines during transportation of gas under cold conditions. The gas hydrate research has grown many interests steadily since 1960. As an alternative energy source, which is also an economical medium for natural gas storage and transportation. The research activities on natural gas hydrates based on publications, subject area, and countries are summarized in Figure 2.2. After several field test activities done around 1995 there has been an exponential growth on the research publications over the past 20 years from different subject area (Cai *et al.*, 2016).

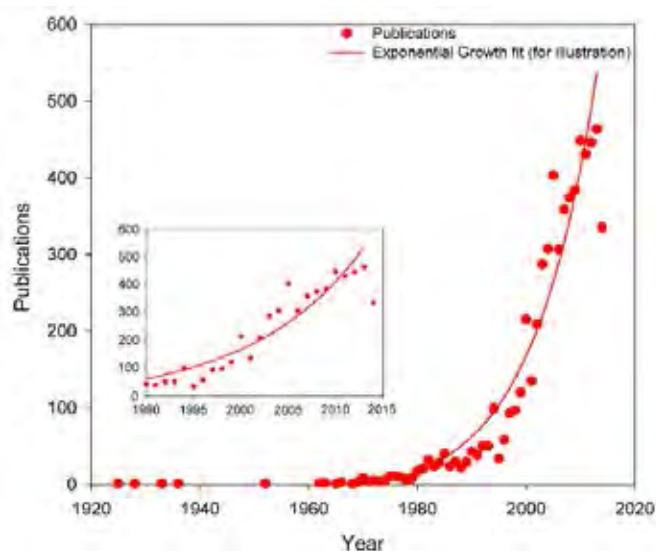


**Figure 2.2** Progress of research activity on “natural gas hydrates” or “methane hydrates” (data obtained from Scopus database on 03-October-2014, data presented till the year 2013) (Chong *et al.*, 2016).

Hydrates form from water and non-stoichiometric amounts of small non-polar molecules under moderate pressure and at low temperatures typically close to 0 °C. However, they burn easily in the barometric pressure. If methane hydrates are either warmed or depressurized, they will revert back to water and gas. Figure 2.3 demonstrates methane hydrates releasing by lighting a match. The heat from the

match will cause the hydrate to dissociate, and the methane molecules will be ignited as they are releasing.



**Figure 2.3** Methane hydrate dissociation with the methane ignited (www.news.nationalgeographic.com).

There are three main structures of gas hydrates, cubic structure I (sI), cubic structure II (sII), and the hexagonal structure (sH). As shown in Table 2.1, the different gas hydrate structures are based on a number of cavities and water molecules. The water cages are described by the general notation  $X^n$ , where  $X$  is the number of sides of a cage face, and  $n$  is the number of cage faces having these  $X$  sides. For example  $5^{12}6^2$  means that a cage is formed by 12 five membered rings and 2 six membered rings.

**Table 2.1** Properties of different hydrate structures (Sloan *et al.*, 1998b)

Hydrate Crystal Structures	I		II		H		
	<u>Small</u>	<u>Large</u>	<u>Small</u>	<u>Large</u>	<u>Small</u>	<u>Medium</u>	<u>Large</u>
Cages(cavity) size							
Description	$5^{12}$	$5^{12}6^2$	$5^{12}$	$5^{12}6^4$	$5^{12}$	$4^35^66^3$	$5^{12}6^8$
Cages per unit cell	2	6	16	8	3	2	1
Average cavity radius(Å)	3.95	4.33	3.91	4.73	3.94	4.04	5.79
Water molecules per cell	46		136		34		



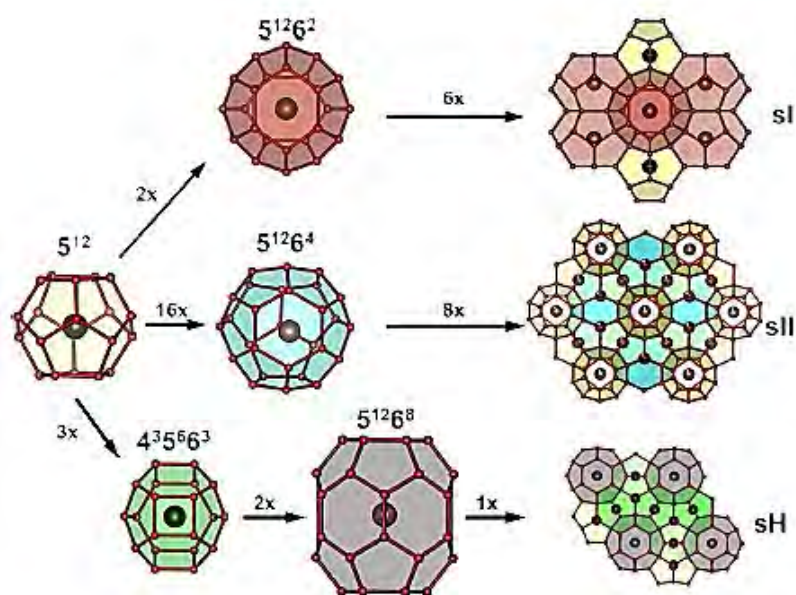


**Figure 2.4** Three most common hydrate structures, sI, sII, sH, and the number of cages, which make up their respective unit cells (Grim, 2014).

Figure 2.4 shows the gas hydrate structures. The structure of gas hydrates, which are structures-I, II, and H, have been investigated with X-ray diffraction methods (Stackelberg and Müller, 1954; Ripmeester *et al.*, 1987).

The unit cell of structure-I (sI) is a 12 Å cube consisting of 46 water molecules, which has two types of cavities. The two small cavities are pentagonal dodecahedra ( $5^{12}$ ), whereas the six large cavities are tetradecanahedra ( $5^{12}6^2$ ) having two opposite hexagonal faces and twelve pentagonal faces. The smaller cavities are almost spherical, whereas the larger cavities of structure-I are slightly oblate. While the unit cell of structure-II (sII), which is a 17.3 Å cube with 136 water molecules, also contains two types of cavities. The 16 smaller cavities are distorted pentagonal dodecahedra and the 8 larger cavities are hexadecanahedra ( $5^{12}6^4$ ) having 4 hexagonal faces and twelve pentagonal faces. The latter cavities are almost spherical in shape (Stackelberg and Müller, 1954). The Structure-H has three  $5^{12}$  cavities, which is common to all known hydrate structures and two new 12 faces  $4^3 5^6 6^3$  cavities and one new large  $5^{12}6^8$  cavity. The  $4^3 5^6 6^3$  cavity has three square faces, six pentagonal

faces, and three hexagonal faces, whereas the  $5^{12}6^8$  cavity has 12 pentagonal faces and eight hexagonal faces (Ripmeester *et al.*, 1987).

## 2.2 Gas Hydrates Properties

Water molecules of hydrates are linked through hydrogen bonding to create cavities that can enclose a large variety of molecules (guests). No chemical bonding takes place between the host water molecules and the enclosed guest molecule. According to the hydrate model, the water molecules form defined crystal lattice (the host lattice), which contains small gas molecules (guests). The adsorption energy may reduce the free energy of the hydrates sufficiently to make the hydrate which more stable than pure water. The mechanical properties of hydrate structures are shown in Table 2.

**Table 2.2** Comparison of properties of ice, sI, and sII hydrate crystal structures (Demirbas, 2010)

Property	Ice(I <sub>h</sub> )	Structure I	Structure II
Water molecules number	4	46	136
Lattice parameters at 273 K, nm	a = 0.452 c = 0.736	1.20	1.73
Dielectric constant at 273 K	94	~58	58
Water diffusion correlation time, $\mu$ s	220	240	25
Water diffusion activation energy, kJ/m	58.1	50	50
Isothermal Young's modulus at 268 K, $10^9$ Pa	9.5	8.4(est.)	8.2(est.)
Poisson's ratio	0.33	~0.33	~0.33
Bulk modulus (272 K)	8.8	5.6	NA
Shear modulus (272 K)	3.9	2.4	NA
Compressional velocity( $V_p$ ), m/s	3870.1	3778.0	3821.8
Shear velocity( $V_s$ ), m/s	1949	1963.6	2001.1
Velocity ratio (comp./shear)	1.99	1.92	1.91
Linear thermal expn., at 200 K, $K^{-1}$	$56 \cdot 10^{-6}$	$77 \cdot 10^{-6}$	$52 \cdot 10^{-6}$
Adiab. Bulk compress. (273 K), $10^{-11}$ Pa	12	14(est.)	14(est.)
Heat Capacity, $J \text{ kg}^{-1} \text{ K}^{-1}$	3800	3300	3600

The following properties of sI and sII are determined by the molecular structure, described by three heuristics: (i) Mechanical properties compared those of ice. In addition, hydrates are 85 mol% water for each volume. The hydrates may contain large volumes of the hydrate-forming species at standard temperature and pressure conditions (STP). (ii) Phase equilibrium is set by the size ratio of guest molecules within host cages. The three-phase equilibrium pressure (liquid water-hydrate-vapor; L<sub>w</sub>-H-V) depends on exponentially temperature. (iii) Heats of formation are set by the hydrogen-bonded crystals and are reasonably constant within a range of guest sizes (Sloan, 1998a).

The physical properties of gas hydrates trapped in sediments are very important for detecting the presence of these compounds, estimating the amount of gas hydrates trapped in the sediments, and developing processes to exploit this resource (Jorge and Gabitto, 2010). The laboratory and analytical investigations showed the results that the physical properties of the sediments such as the bulk densities of methane hydrates were ranged from 0.35 to 0.75 kg/L, and methane hydrates were inversely correlated with the pore volume ranging from 10% to 70% by volume.

Some experiments showed the anomalous preservation of methane hydrates at temperatures below 273 K at ambient pressure. They also showed that simultaneous formation of ice phase at temperatures above 242 K can affect the preservation up to 93% of methane. This resulted in possible applications of this effect for production, storage, and transportation of natural gas. In addition, the pressure of methane hydrates for decomposition was about 13 bars at 250 K. The unusual behavior of some gas hydrates upon heating occurred. It was found that the density in the hydrate phase was larger than in the ice phase. A series of empirical expressions for predicting gas hydrate stability, gas hydrate volume fraction out of pore space, and gas hydrate mass-density were established in different systems with different gas composition (CH<sub>4</sub>, C<sub>2</sub>H<sub>6</sub>, H<sub>2</sub>S), salinity (NaCl, seawater), and pore size at temperatures between 273.15 and 300 K (Demirbas, 2010).

### 2.3 Methane Hydrates in Natural Resources

In recent years, gas hydrates have been recovered or inferred in many continental margin settings and in onshore permafrost or offshore relict permafrost. As shown in Figure 2.5, gas hydrates have also been recovered from sediments beneath Lake Baikal, Earth's largest freshwater lake.

Biogenic and thermogenic are two main origins of the natural hydrocarbon gases that form natural gas hydrates. Biogenic natural gases are formed from  $\text{CH}_4$ -generating microbes (methanogens) with high methane purity ( $\text{C}_1/\text{C}_{2+} > 100$ ). Another one is thermogenic natural gases that are generated from the decomposition of organic matter from fossil origin.

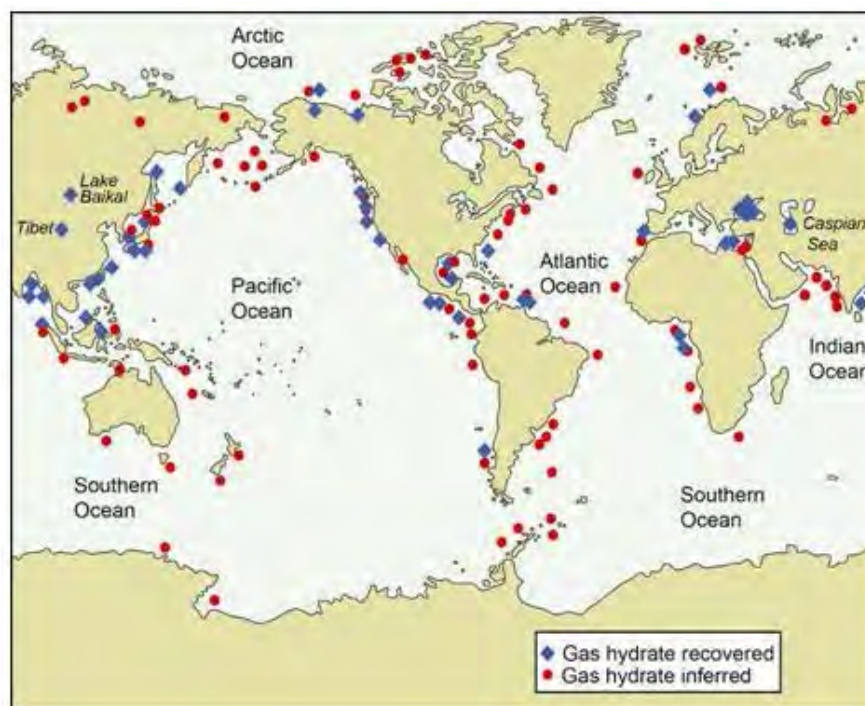


**Figure 2.5** Location of sampled and inferred gas (www7430.nrlssc.navy.mil).

Methane hydrates will most likely be produced first from deposits with the following conditions: 1) the hydrates occur in high concentrations; 2) they occurs in

a high-permeability host rock that has good reservoir quality; and 3) the deposit is located in an area with existing infrastructure.

Most of natural gas hydrates are found in the sI structure. They have been observed in the Gulf of Mexico and Ulleung Basin, the Nankai Trough and South China Sea, and in several other locations. On the contrary, thermogenic natural gas hydrate deposits form the sII or sH hydrate structure and exist at milder conditions, where pure methane does not form hydrates. A recent report also revealed the occurrence of sII hydrates in the permafrost zone of Qilian Mountain (Chong *et al.*, 2016).

## 2.4 Gas Hydrate Formation

Gas hydrate formation is a crystallization process. Nucleation process occurs by dispersion of water and gas clusters that go on until a critically stable sized nucleus has been formed, followed by growth and agglomeration. The visual changes happening to the aqueous liquid contents from the nucleation point till the completion of hydrate formation were continuously recorded by a microscope coupled with a camera connected to the experimental setup. Figure 2.6 shows the images recorded from the nucleation along with the gas uptake for hydrate growth. Square points *A*, *B*, *C*, *D*, *E* and *F* in the hydrate growth curve corresponds to the visual observation images represented as *A*, *B*, *C*, *D*, *E* and *F* below the hydrate growth curve in the figure. After nucleation (induction time, IT), the hydrate growth occurred within the aqueous phase with no change occurring in the gas aqueous liquid interface. Further, the solution remains in well mixed state until about 30 min from induction, which can be seen from uniform white slurry like observation. (Veluswamy *et al.*, 2015).

Moreover, when the hydrates are successfully formed nucleation, a thin hydrates film form on the water–gas interface which grow further in a mass transfer limited regime. It has been identified that the better reactor designs, the higher solubility of hydrate forming guests in water and a larger contact area between the

hydrate formers and water. The well designed reactor can reduce the mass transfer resistance and ensure faster hydrate growth (Kumar *et al.*, 2015).

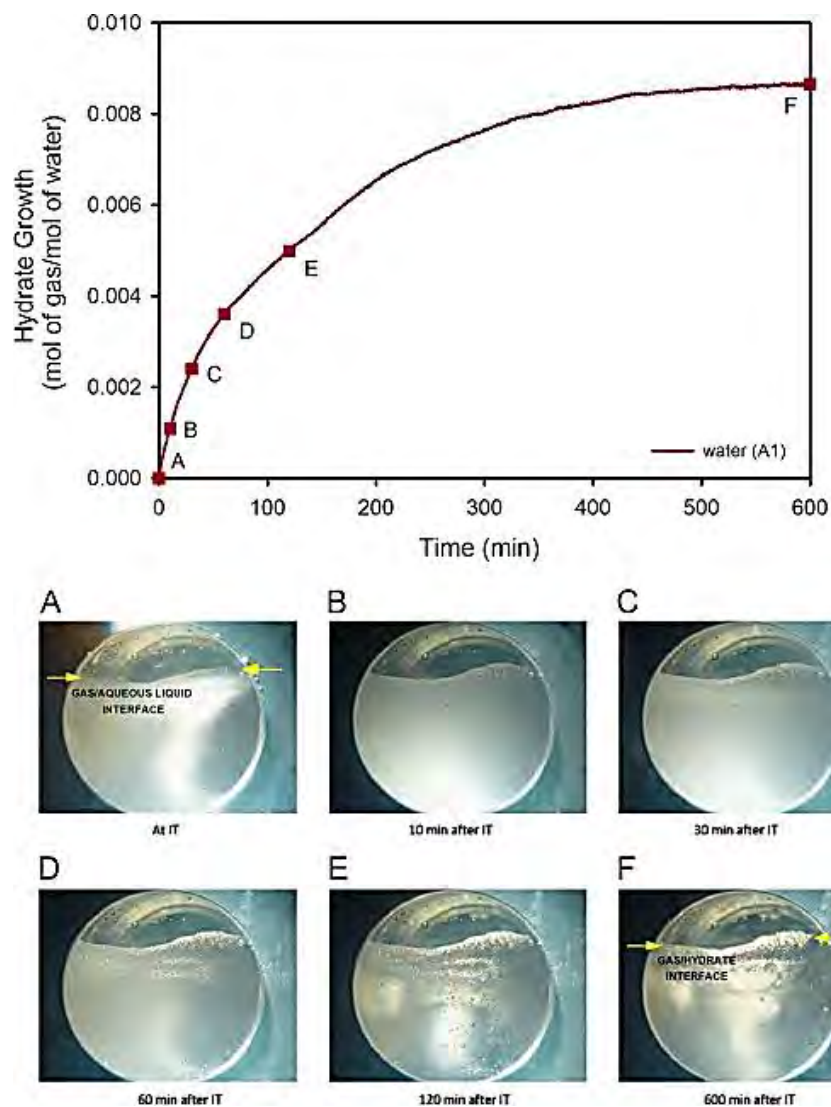


**Figure 2.6** Hydrate growth from nucleation for the mixed hydrogen/propane hydrate formation experiment conducted with water (control experiment; 0 ppm SDS) at 274.2 K and 8.5 MPa (Veluswamy *et al.*, 2015).

## 2.5 Methane Hydrate Stability

Temperature and pressure are the main factors in both formation of gas hydrates and the thickness of the hydrate stability zone. Other factors such as gas

chemistry and gas availability will also alter the thickness and location of the hydrate stability zone. Figure 2.7 shows the phase boundary diagram demonstrated the gas hydrate/freshwater stability field in gray. Boundaries are given for the pure-methane/pure-water system. Directions of hydrate-gas phase boundary shift towards stabilities at higher salinities are indicated by arrows.

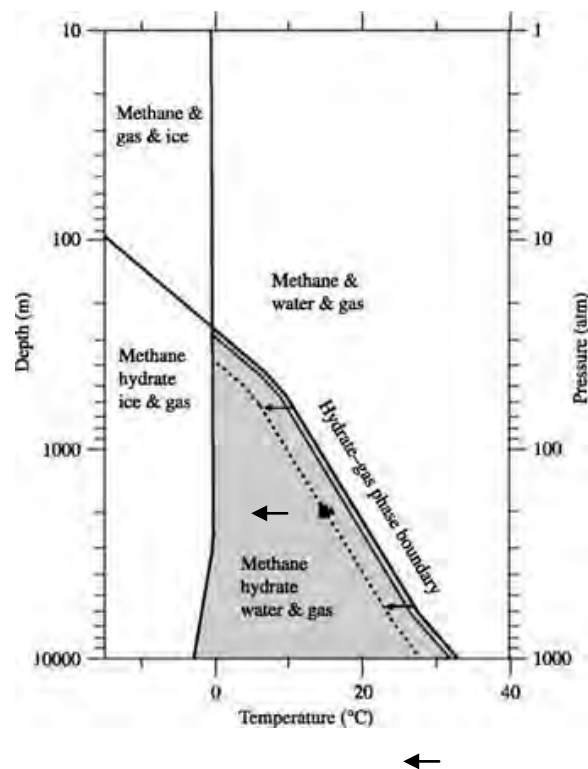


**Figure 2.7** Phase boundary diagram demonstrating the gas hydrate stability field in gray (Demirbas, 2010).

At pressure and temperature outside the hydrate stability range, melting and decomposition of gas hydrates will occur. Decomposition will result in released water and methane gas but requires heat input. As decomposition occurs, the released gas and water create a volume expansion. The decomposition of gas hydrates can show from change in the pressure and temperature regime in the hydrate stability zone and result in a significant volume change. The methane hydrates in the sI structure are much more stable at 1 atm and 268.2 K than other structures, while the sII hydrates are more stable at 1 atm and 268.2-270.2 K (Demirbas, 2010).

## 2.6 Gas Hydrate Dissociation

Depressurization causes the hydrates to dissociate and release methane. Hydrate dissociation is an endothermic process that means the process requires heat. To be successful, a methane hydrate production strategy must include sufficient depressurization to cause the hydrates to dissociate. In some cases, the addition of localized heating overcomes the natural tendency of the hydrates in the reservoir to return to hydrate stability (U.S. Department of Energy, 2011).

There are numerous methods for extracting methane. These methods rely on creating a slow controlled dissociation process, which involves the alteration of the thermodynamic conditions in the hydrate stability zone. The processes will increase the temperature and reduce the pressure. These methods include thermal injection, inhibitor injection, and the depressurization, as shown in Figure 2.8.

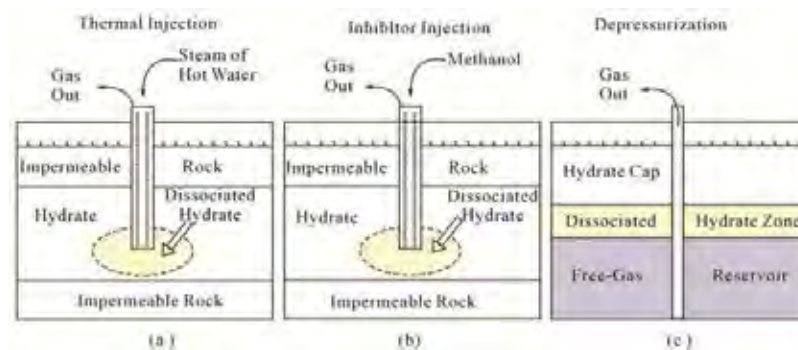


**Figure 2.8** Schematic of gas recovery from gas hydrate methods (Dou *et al.*, 2015).

First of all, the thermal injection method uses relatively hot water or steam injected into a subsea gas hydrate layer, which would partially melt the hydrate beds in ocean sediments or in permafrost regions. The gas will flow to the bore hole, where it can be ascending through the pipe up to the surface. However, the major disadvantage is the heating of the fluids to pump underground would be costly and might not reach deeper hydrate sediments (Archer, 2007).



Second, the inhibitor injection method operates by injecting an organic or inorganic compound that shifts the hydrate equilibrium point to lower temperatures for isobaric conditions with depressurization. The most common thermodynamic organic inhibitors are methanol, monoethylene glycol (MEG), and diethylene glycol (DEG), commonly referred to as glycol, and dissolved salts such as NaCl, CaCl<sub>2</sub>, KCl, and NaBr can also be inhibitors.

Third, the depressurization method is the method that depresses pressure below the stability point causing the hydrate dissociation and the drop in the hydrate temperature. Without an external heat source, depressurization lowers the hydrate temperature to a new equilibrium condition (Demirbas, 2010).

Moreover, there are reports on the thermal behavior of gas hydrates. Some of research works applied thermal methods in recovering gas from hydrates for example thermal stimulation in the laboratory scale achieved by hot water injection, water bath immersion to temperatures above hydrate equilibrium point (Chong *et al.*, 2016).

## **2.7 Physical Chemistry of Methane Hydrates**

### **2.7.1 Thermodynamics**

Thermodynamically, the stability of hydrates is determined by the temperature and the availability of methane. The partial pressure of methane is determined by the total fluid pressure. At atmospheric pressure, hydrates are not stable at earth surface temperature. At water depths of 100 m, hydrates would form at about  $-20$  °C. While at 500 m depth, the melting temperature approaches *in-situ* temperatures. This minimum stability depth is somewhat shallower in the high-latitude oceans about 200 m in the arctic ocean (Archer, 2007).

### **2.7.2 Kinetics**

Hydrates can persist metastable. In general, kinetic effects are probably of secondary importance for predicting the hydrate response to anthropogenic climate change because the thermal force takes place on such long time scales. Lab experiments show that hydrates can nucleate from the pure aqueous

phase with no bubbles required. Several studies predict inhibition of hydrate formation in fine grained sediment caused by the high activation energy. This can explain that the characteristic textures of hydrates that hydrates should form first or predominantly in sandy sediments (Winters *et al.*, 2004).

## 2.8 Natural Gas Hydrate Transportation

Gas can be transported as a solid, with the solid being gas hydrates. Natural gas hydrates (NGH) are the product of mixing natural gas with liquid water to form a stable water crystalline ice like substance. The transportation of NGH is believed to be a viable alternative to LNG or pipelines for the transportation of natural gas from source to demand. The hydrates are considered an excellent way of transportation and storage natural gas in large quantities. The transportation cost is expected to be 18–24% lower than with liquefied transportation. Gas storage in the hydrate form also becomes especially efficient at relatively low pressures, where substantially more gas per unit volume is contained in the hydrates than in the free state when the pressure is dropped. The lower cost difference, the simplicity, and flexibility of the process should be required. Figure 2.9 shows the methane hydrate chain consists of three main parts, which are the production, marine transportation, and regasification. The production part can be located on land using the loading facilities for large hydrate carriers. Transportation is performed by bulk carriers specially designed for dry hydrates, hydrate slurries, and pellet type hydrates (Kim *et al.*, 2010).

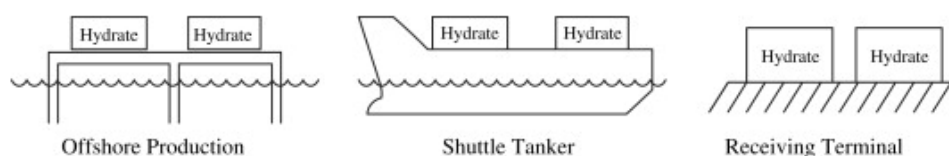


**Figure 2.9** Hydrate transportation chain (Kim *et al.*, 2010).

The hydrates can be stored at normal temperatures (0-10 °C) and pressures (10 to 1 atmosphere), where 1 m<sup>3</sup> of hydrates should contain about 160 m<sup>3</sup> gas per

$\text{m}^3$  of water. This concentration of gas is attractive as it is easier to produce, safer, and cheaper to store compared to the  $200 \text{ sm}^3$  per  $1 \text{ m}^3$  of compressed gas (high pressure  $>3,000$  psig) or the  $637 \text{ sm}^3$  gas per  $1 \text{ m}^3$  of LNG (low temperatures of  $-162$  °C) (Thomas and Dawe, 2003).

## 2.9 Promotion of Gas Hydrate Formation

In recent years, the gas hydrates play more important roles in industrial systems and draw much attention as a subject of engineering studies. Gas hydrates can form at high pressure and temperatures above  $273 \text{ K}$  conditions. Due to the formation conditions, one of the possible methods is to add additives in water, such as CP, TBPB, and TBAB. Many researches study in two types of additives. One is the additives, which can promote the formation of gas hydrates by shifting the phase equilibrium curve toward lower pressure and higher temperature conditions, are called thermodynamic promoters. The other additives, which can increase the rate of hydrate formation, are called kinetic promoters (Godishala *et al.*, 2013).

In hydrate structures, a cage like network is formed by hydrogen bonded water molecules, in which the guest molecule is surrounded. In addition, hydrates can form semihydrate structures, which are guest–host crystalline compounds that share many similarities with hydrates, and are composed of water (host) and hydrocarbons hydrophobic substances (guest). Compounds that induce semihydrate formation also form a part of the cage-lattice that is surrounded by the water molecules. Therefore, semi hydrates forming compounds can be regarded as both guest and host components. Salts containing the tetra-n-butylammonium (TBA) or phosphonium (TBP) cation have a strong tendency to form semiclathrates because the cations fit into the hydrate cage excellently (Muromachi *et al.*, 2014).

### 2.9.1 Tetra-n-butylphosphonium Bromide (TBPB)

Tetra-n-butylphosphonium bromide (TBPB) is a positively charged compound with the formula  $\text{C}_{16}\text{H}_{36}\text{BrP}$ . The structure of TBPB contains n-butyl

hydrocarbon groups connected with phosphonium ion. Figure 2.10 shows the structure of TBPB ([www.chemicalbook.com](http://www.chemicalbook.com)).



**Figure 2.10** Structure of TBPB (<http://www.chemicalbook.com>).

### 2.9.2 Tetra-n-butylammonium Bromide (TBAB)

Tetra-n-butylammonium bromide (TBAB) is a compound with the formula  $C_{16}H_{36}BrN$ . The structure of TBAB contains n-butyl hydrocarbon groups connected with ammonium ion. Figure 2.11 shows the structure of TBAB ([www.chemicalbook.com](http://www.chemicalbook.com)).

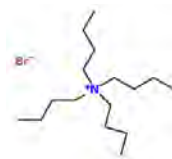


**Figure 2.11** Structure of TBAB (<http://www.chemicalbook.com>).

### 2.9.3 Cyclopentane (CP)

Cyclopentane (CP) consists of a ring of five carbon atoms each bonded with two hydrogen atoms with chemical formula  $C_5H_{10}$ . It occurs as a colorless liquid with a petrol like odor. Figure 2.10 shows the structure of CP ([www.chemicalbook.com](http://www.chemicalbook.com)).



**Figure 2.12** Structure of CP (<http://www.chemicalbook.com>).

Wang *et al.* (2015) studied the effects of anionic surfactants on methane hydrate formation. Three anionic surfactants with the same carbon chain but different head groups, sodium dodecyl sulfonate (SDSN), sodium dodecyl sulfate (SDS), and sodium dodecyl benzene sulfonate (SDBS), were used. The result showed that the contact angles of surfactant solutions on the reactor sidewall affected the hydrate growth pattern. Figure 2.13 shows that increasing in the SDBS concentration increased micelle concentration and consequently shortened the induction time. Moreover, hydrates grew upwards on the reactor sidewall in the hydrate formations with SDSN and SDS due to the narrow contact angles, while when SDBS was used, hydrates mainly formed in the bottom of the reactor because of the wide contact angles.

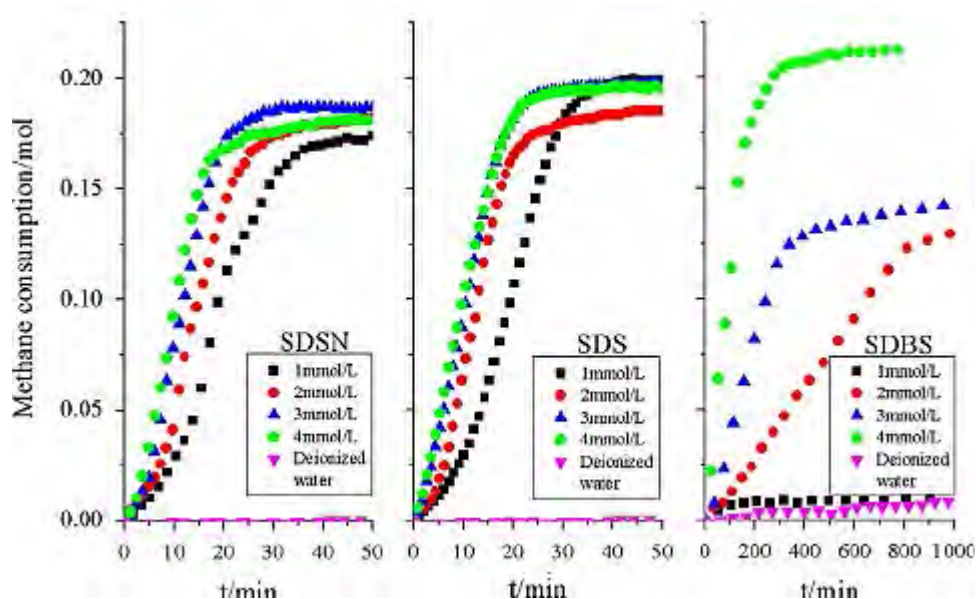


**Figure 2.13** The evolutions of the methane consumption during the hydrate growth period (the initial pressure was 6 MPa, the temperature was 275.15 K and the water was 1.67 mol) (Wang *et al.*, 2015).

Verrett *et al.* (2012) investigated the effects of sodium dodecyl sulfate (SDS) for promoting hydrate growth. The bulk liquid phase hydrates were formed in a stirred 600 cm<sup>3</sup> isobaric/isothermal reactor containing 343 cm<sup>3</sup> of liquid. Bulk

solubility experiments under hydrate–liquid, liquid–gas, and hydrate–liquid–gas equilibrium were performed at temperatures ranging from 275.1 K to 283.3 K and pressures ranging from 3,049 kPa to 6500 kPa with pure water and SDS solutions. The result indicated that SDS had no effect on bulk methane solubility but SDS did affect the methane mole fraction in the bulk liquid during the hydrate growth. The increase in the hydrate growth rates was measured through gas consumption and compared to the increase in the driving force for hydrate formation.

Aliabadi *et al.* (2015) studied CuO nanoparticles as a new nanoparticle to investigate the effect of this nanoparticle concentration on the gas hydrate formation. They also studied the effects of pressure and SDS concentration on the gas hydrate formation. The result showed that 500 ppm of surfactant (SDS) led to the good stability of the solution within five days. The optimal concentration of nanoparticles in the solution at the temperature of 2.5 °C was 10 ppm. The induction time decreased significantly to 14 min because CuO nanoparticles provided suitable locations for the heterogeneous nucleation of gas hydrate crystals. The induction time decreased about 92.7% compared to the pure water system. Figure 2.14 shows the gas hydrate induction time variations with the initial pressure.

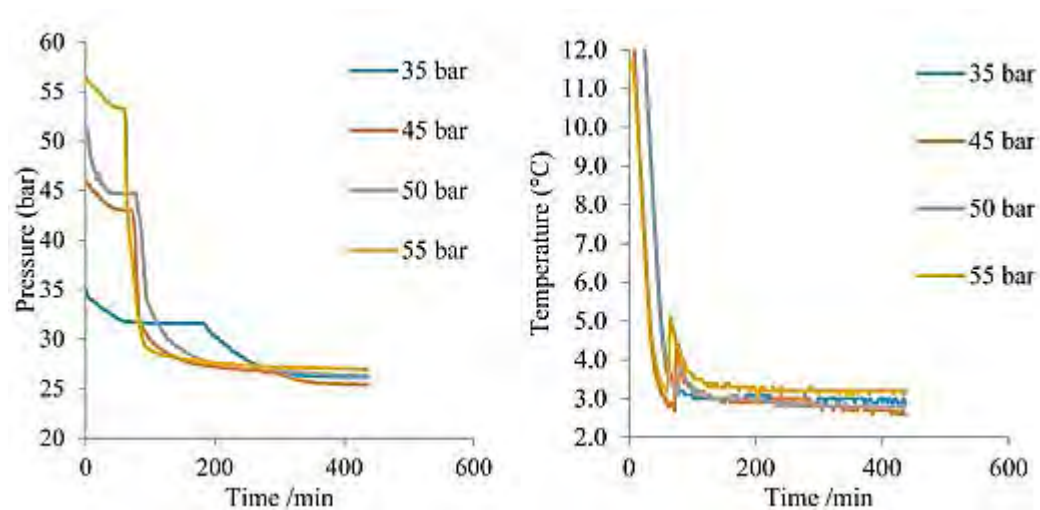


**Figure 2.14** The gas hydrate induction time variations with the initial pressure (Aliabadi *et al.*, 2015).

Babakhani and Alamdari (2016) investigated the effects of maize starch on the methane hydrate formation/dissociation rates and stability. Results showed that the maize starch at low concentrations had no significant effect on the hydrate formation rate but, at the high concentrations of 600, 800, and 1000 ppm, the maize starch increased the formation rate. The 800 ppm of maize starch concentration, increased the hydrate formation rate up to 2.5 times compared to no maize starch at the same conditions. Moreover, results showed that the stability at minus 4 °C was less than that at minus 1 °C. Figure 2.13 shows the dissociation of hydrates at subzero temperatures is in the range 2-5%, and the minimum instability is observed at the 800 ppm maize starch concentration. However, self-preservation phenomenon prevented instability. Some dissociation about 4-5% occurred before complete self-preservation.

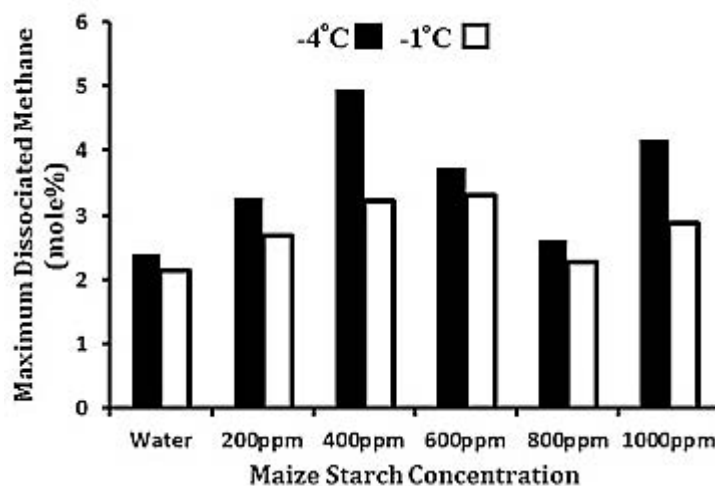


**Figure 2.15** Maximum dissociated methane as mole percent for different maize starch concentrations at temperatures minus 4 °C and minus 1 °C (Babakhani and Alamdari, 2015).

Mech *et al.* (2015) investigated the experimental data for the phase equilibrium of methane hydrates in the presence of THF (0.005 and 0.01 mass fraction) and TBAB (0.1 and 0.2 mass fraction) with various inhibitors. Various inhibitors used in their study included sodium chloride (NaCl), methanol (MeOH)

and ethylene glycol (EG) with mass fraction (0.03 and 0.1) of each inhibitor in the aqueous solutions of THF and TBAB. Moreover, comparative effects of NaCl, MeOH and EG on hydrate/semihydrates of  $\text{CH}_4 + \text{H}_2\text{O} + \text{THF/TBAB}$  were studied. The inhibition effect of NaCl on the hydrates of  $\text{CH}_4 + \text{H}_2\text{O} + \text{THF}$  was observed to be higher than MeOH and EG whereas, for semihydrate,  $\text{CH}_4 + \text{H}_2\text{O} + \text{TBAB} + \text{MeOH}$  was observed to be an effective inhibitor than NaCl and EG. In addition, as the concentration of promoters (THF and TBAB) increased, the effect of inhibitors is decreased. This indicated that lower concentrations of promoters along with inhibitors may be suitable for efficient formation and dissociation of natural gas storage and transportation.

Muromachi *et al.* (2014) studied the crystal structure analysis of the semi hydrates of TBPB to develop a more precise model. In their study, the chemical formula of the crystal was determined to be  $\text{TBPB} \cdot 38\text{H}_2\text{O}$ . Figure 2.16 illustrates the unit cell of the TBPB hydrates. This structural preference may account for the relatively high gas capacity of the TBPB hydrates due to the difference in the ratio of water molecules to the cages, which can be occupied by the guest gas. The structure features three dodecahedral cages for each TBPB molecule that may accommodate small gas molecules such as  $\text{CH}_4$ ,  $\text{CO}_2$  and  $\text{N}_2$ .

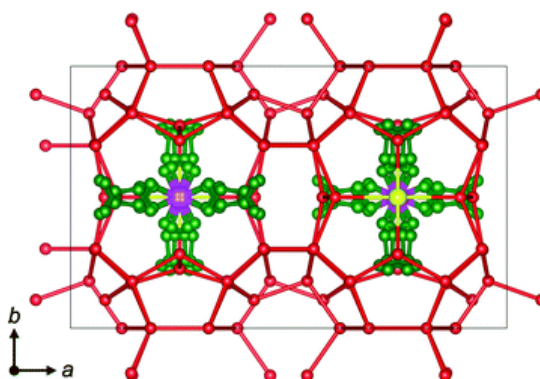


**Figure 2.16** Unit cell of the presently found TBPB hydrate crystal. Atom types are denoted as follows: green: carbon; red: oxygen; pink: phosphorus; yellow: bromine. Hydrogen atoms are omitted for clarity (Muromachi *et al.*, 2014).



Suginaka *et al.* (2012) studied the thermodynamic properties of ionic semihydrate formed with TBPB by the measurements of temperature composition phase diagram, dissociation enthalpy, and visual observation of the hydrate crystal. The hydrate crystal growth and oligo crystals of TBPB are shown in Figure 2.17 at  $T_{\text{ex}} = 281.2$  K and  $w_{\text{TBPB}} = 0.35$ . Crystal samples in the size of 0.3-0.5 mm were cut from the oligo crystals and then subjected to the single-crystal X-ray diffraction measurements. In their study, the result showed that the highest equilibrium temperature for TBPB system was 282.4 K in the mass fraction range from 0.33 to 0.35. From the measurements of dissociation enthalpy of the TBPB hydrate, the highest dissociation enthalpy was 214 kJ/kg at  $w_{\text{TBPB}} = 0.35$ .

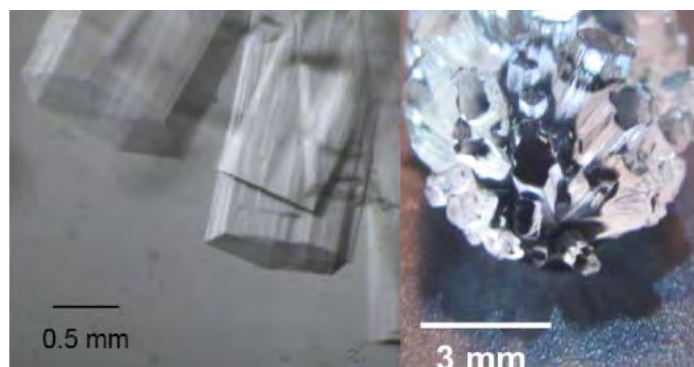


**Figure 2.17** Hydrate crystal growth and oligo crystals of TBPB at  $w_{\text{TBPB}} = 0.35$  and  $T_{\text{ex}} = 281.2$  K (Suginaka *et al.*, 2012).

Du *et al.* (2015) studied the pressure requirement for the hydrate formation of simulated mine ventilation air (MVA) (0.5 vol%  $\text{CH}_4$  + 99.5 vol% air) in the presence of tri-n-butyl phosphine oxide (TBPO) or TBAB at three different initial loadings (5 wt%, 15 wt%, and 26 wt%). The phase equilibrium conditions of hydrates formed by TBAB or TBPO were measured in the temperature range of 277.61-295.54 K and pressure range of 0.2-19.1 MPa. The results indicated that the effect of promoters on reducing the pressure for MVA hydrate formation followed the order of TBPO > TBPB > TBAB. The highest methane enrichment ratio obtained in this work was 300% with TBPO at initial loading of 5 wt%.

Du *et al.* (2014b) measured phase equilibrium conditions for the hydrates formed from simulated MVA (0.50 vol% CH<sub>4</sub> + 99.50 vol% air) in the presence of 0, 5, 20, 37.1, and 50 wt% of TBPB. It was found that the addition of TBPB moved the MVA hydrate equilibrium conditions to higher temperatures and lower pressures. The results showed that addition of TBPB allowed the hydrate dissociation condition for mine ventilation air to become milder, and at a given temperature, the lowest hydrate dissociation pressure was achieved at 37.1 wt% TBPB, corresponding to the stoichiometric composition for TBPB·32H<sub>2</sub>O. CH<sub>4</sub> was also preferentially incorporated into the hydrate phase, and the enrichment was approximately 3.5-fold in the hydrate phase.

Shi *et al.* (2013) investigated the phase equilibrium conditions for semihydrates formed in systems of TBPB + CO<sub>2</sub> + H<sub>2</sub>O and TBPB + N<sub>2</sub> + H<sub>2</sub>O. The experiments were performed in the temperature range of 282.2-292.0 K and in the pressure range of 1.32-16.856 MPa with TBPB aqueous solutions of 0.050, 0.100, 0.371, and 0.600 mass fraction. The result shows that the strongest stabilization effect was observed with the presence of TBPB aqueous solution of 0.371 mass fractions. Corresponding to the stoichiometric composition for TBPB·32H<sub>2</sub>O, the presence of TBPB caused the phase equilibrium lines of CO<sub>2</sub> or N<sub>2</sub> hydrates to be greatly shifted to a stabilized region represented by higher temperature and lower pressure.

Deschamps and Dalmazzone (2010) studied the dissociation temperatures of hydrogen + TBAB, tetrabutylammonium chloride (TBACl), and TBPB. The semihydrates were measured using differential scanning calorimetry under pressure. In their work demonstrates that the dissociation temperatures of H<sub>2</sub> + TBACl and H<sub>2</sub> + TBPB semihydrates are very close to ambient at low pressures around 15.0 MPa. The result showed that mass fraction deduced from the ratio (nH<sub>2</sub>/nH<sub>2</sub>O). The system of H<sub>2</sub> + TBACl and H<sub>2</sub> + TBPB semi hydrates can store 0.12% and 0.14% of hydrogen.

Wang and Dennis (2015) determined the formation temperature of TBAB, tetrabutylammonium fluoride (TBAF) and TBPB semihydrates and provided the phase equilibrium data of TBA<sup>+</sup> and TBP<sup>+</sup> semihydrates formation. The formation

temperature of all hydrates peaked around a value of 30 wt% for TBAF, 35 wt% for TBAB and 35 wt% for TBPB, and the induction time of TBPB hydrates slightly increased as the SDS mass fraction rised, as shown in Figure 2.18. Moreover, the induction time in the 1<sup>st</sup> formation was usually much longer than that in the repeated formations.

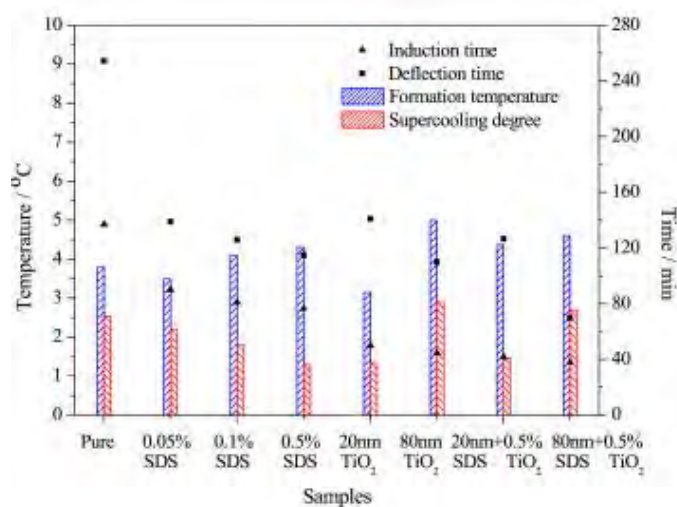


**Figure 2.18** 25 wt% TBPB hydrate formation of semihydrates with different additives (Wang and Dennis, 2015).

Li *et al.* (2007) studied hydrate dissociation conditions in the presence of CH<sub>4</sub>+TBAB+water. The three phase equilibrium lines obtained in the present study were shifted to the low temperature or high pressure side from that of the stoichiometric TBAB solution. Figure 2.19 shows the addition of TBAB caused the hydrate equilibrium pressure to be drastically lowered by 52 to 96% at a specified temperature. The hydrate equilibrium temperature rose by about 4 to 17 K at a specified pressure depending on the component of TBAB in water. Methane uptake into semihydrates were confirmed by a shift in the hydrates regions when TBAB was present.

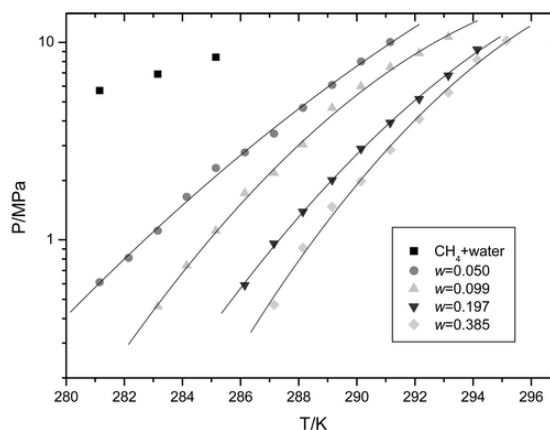


**Figure 2.19** Hydrate dissociation for  $\text{CH}_4 + \text{TBAB} + \text{water}$  (Li *et al.*, 2007).

Ye and Zhang (2014) studied the phase equilibrium data of TBPB hydrates with and without  $\text{CO}_2$  at mass fractions are 0.10, 0.20, 0.35, and 0.50 in the pressure range of 0.4 to 4.0 MPa and in the temperature range of 281.0 to 292.0 K. the crystal morphologies of TBPB hydrates with and without  $\text{CO}_2$  are visually observed. Figure 2.20 shows a sequence of photos of  $\text{CO}_2 + \text{TBPB}$  double hydrate crystals growing in TBPB aqueous solution at  $w = 0.10$ ,  $\Delta T_{\text{sub}} = 4.5$  K, and  $p = 2.950$  MPa. in Figure 2.20a shows the early stage of hydrate crystal formation at 180 second until a lot of  $\text{CO}_2 + \text{TBPB}$  double hydrate crystals in columnar shape appear. No plate shaped crystals are observed anymore. At 2220 second are shown in Figure 2.20b. The large proportion of  $\text{CO}_2 + \text{TBPB}$  double hydrate crystals are in a columnar shape which is similar to the case of  $\text{CO}_2 + \text{TBAB}$  double hydrate crystals as shown in Figure 2.20c. At 6120 second undefined shapes composed of small thin crystals as shown in Figure 2.20d. At  $w = 0.10$ , the phase equilibrium data of  $\text{CO}_2 + \text{TBPB}$  double hydrate are almost consistent with those of  $\text{CO}_2 + \text{TBAB}$  double hydrate, but there is a difference between them at  $w = 0.20$  in high pressure range.

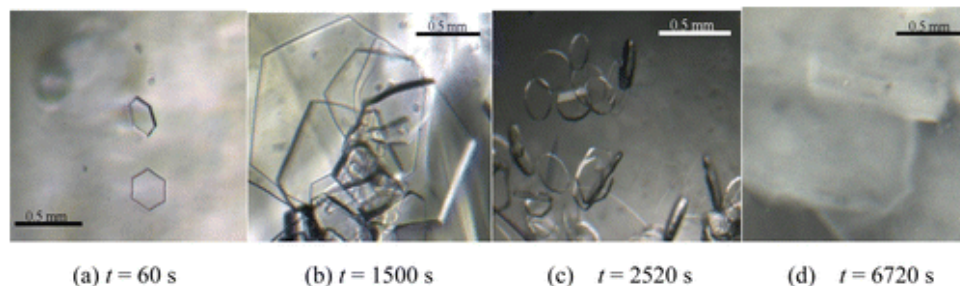


**Figure 2.20** Sequential photos of the growth of TBPB semihydrates crystals at  $w = 0.10$ ,  $\Delta T_{\text{sub}} = 4.7$  K at atmospheric pressure (Ye and Zhang, 2014).

Wang and Dennis (2016) determined enthalpy and heat capacity of semihydrates data of TBAF, TBAB and TBPB. The results showed that enthalpy and heat capacity of TBAF + TBPB semihydrates at a mass fraction of 30 wt% was considered the most suitable for air conditioning cold storage among all candidates. The formation temperature (or freezing point) of single/binary TBAF semihydrates as a function of mass fraction determined in the previous study is in Figure 2.21. The red area in Figure 2.21 is marked as the suitable temperature range for conventional air conditioning applications about 5-12 °C.

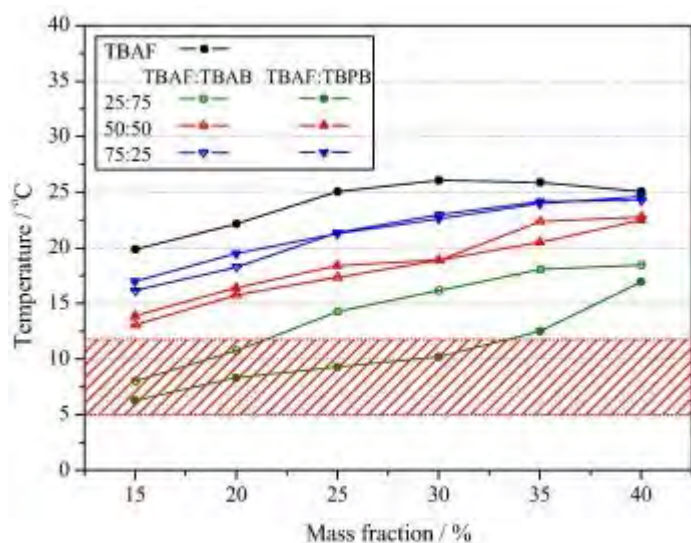


**Figure 2.21** Formation temperature of single/binary TBAF hydrate (Wang and Dennis, 2016).

Iino *et al.* (2014) studied the conditions for the semihydrates formed in the following three systems,  $O_2 + \text{TBPB} + \text{water}$  system,  $\text{CH}_4 + \text{TBPB} + \text{water}$  system, and  $\text{N}_2 + \text{TBPB} + \text{water}$  system. In their study, three phase equilibrium conditions (liquid + hydrate + vapor) was determined between 282.6 and 291.6 K, and 0.15–5.10 MPa with TBPB solution of  $w_{\text{TBPB}} = 0.35$ . The system with  $\text{CH}_4 + \text{TBPB} + \text{water}$  system was shown in Figure 2.22. The results indicated that where the equilibrium pressure at a given temperature was lower in the order of  $\text{CO}_2$ ,  $\text{CH}_4$  and  $\text{N}_2$ . This further indicated the possibility of capturing  $\text{CO}_2$  from the  $\text{CH}_4 + \text{CO}_2$  and  $\text{N}_2 + \text{CO}_2$  mixtures. The range of the equilibrium temperature was from 282.6 K on the lower side to 291.6 K on the higher side.

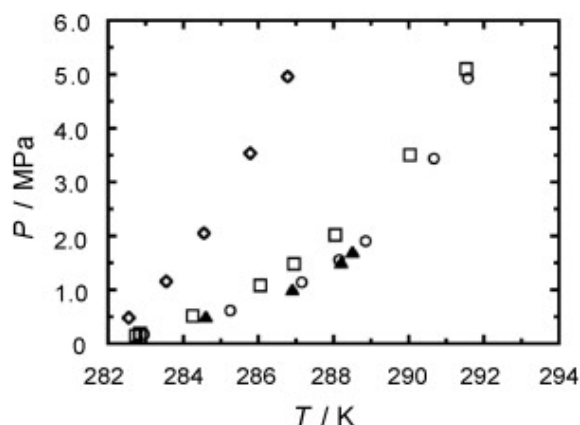


**Figure 2.22** Equilibrium  $P$  versus  $T$  condition for three phase involving hydrate in TBPB containing systems: ○,  $O_2 + \text{TBPB} + \text{water}$  system; ▲,  $\text{CO}_2 + \text{TBPB} + \text{water}$  system; □,  $\text{CH}_4 + \text{TBPB} + \text{water}$  system; ◇,  $\text{N}_2 + \text{TBPB} + \text{water}$  system. The mass fraction or mole fraction of TBPB in the solution  $w_{\text{TBPB}} = 0.35$  (Iino *et al.*, 2014).

Zheng *et al.* (2017) studied effects of CP on  $\text{CO}_2$  hydrate formation and dissociation with different molar ratios of CP/water (0, 0.0025, 0.005, 0.0075, 0.01, 0.02, and 0.03). The results indicated that 0.01 molar ratios of CP/water be used as the optimal case of a thermodynamic promoter in the  $\text{CO}_2$  hydrates in the presence of a salt solution. Increased in the CP concentration significantly decreased the  $\text{CO}_2$  hydrate equilibrium pressure.

Lim *et al.* (2013) investigated morphology of carbon  $\text{CO}_2$ -CP hydrates with or without SDS. They presented the mechanism of the  $\text{CO}_2$ - $\text{H}_2$ -CP system in an unstirred system, as shown in Figure 2.23. The nucleation and formation of hydrates took place at the CP-water interface. The hydrates grew upward in the gas mixture along the crystallizer walls first before penetrating into the water layer. During the downward growth of hydrates, the water layer could be seen to decrease rapidly. In addition, the gas uptake for 0.9 mL of CP was 2.3 times higher compared to the gas uptake for 0.45 mL of CP experiment at 275.65 and 277.65 K.

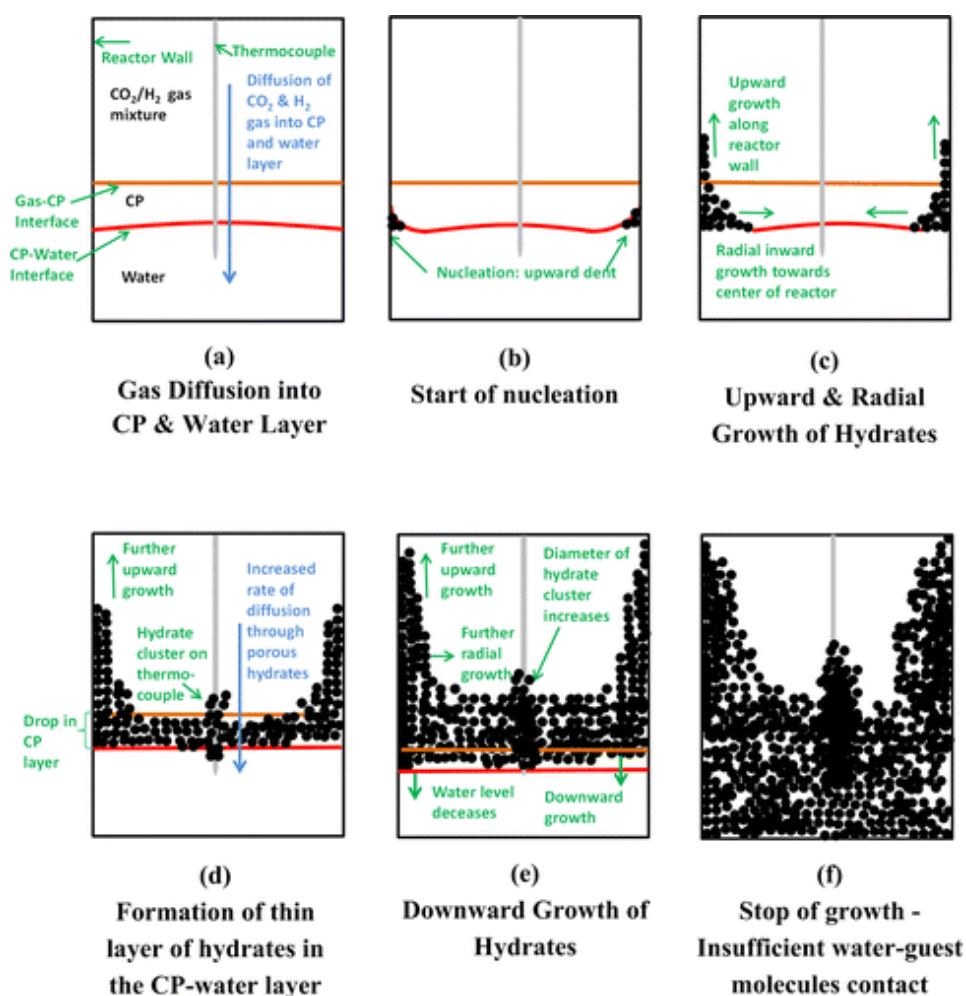


**Figure 2.23** Pictorial illustration of the mechanism of  $\text{CO}_2$ - $\text{H}_2$ -CP hydrates in an unstirred system (Lim *et al.*, 2013).

Li *et al.* (2012a) studied synergic effect of CP and TBAB on hydrate based CO<sub>2</sub>. The CP with CP/TBAB solution ratio of 5 vol% added into the 0.29 mol% TBAB solution can remarkably increase the gas uptake at 4.0 MPa and 274.65 K. Figure 2.24 shows the gas uptake profiles for the different systems with the same feed gas of the component of 38.6 mol% CO<sub>2</sub> and balanced H<sub>2</sub> vs time. They proposed that the CP molecules housed in the hollow centers of the large cavities together with TBAB cation (TBA<sup>+</sup>) make the semihydrate structure more stable. More TBAB participating in forming the semihydrate containing CP, TBAB and mixture gas, and further led to the remarkable increase of the gas uptake.

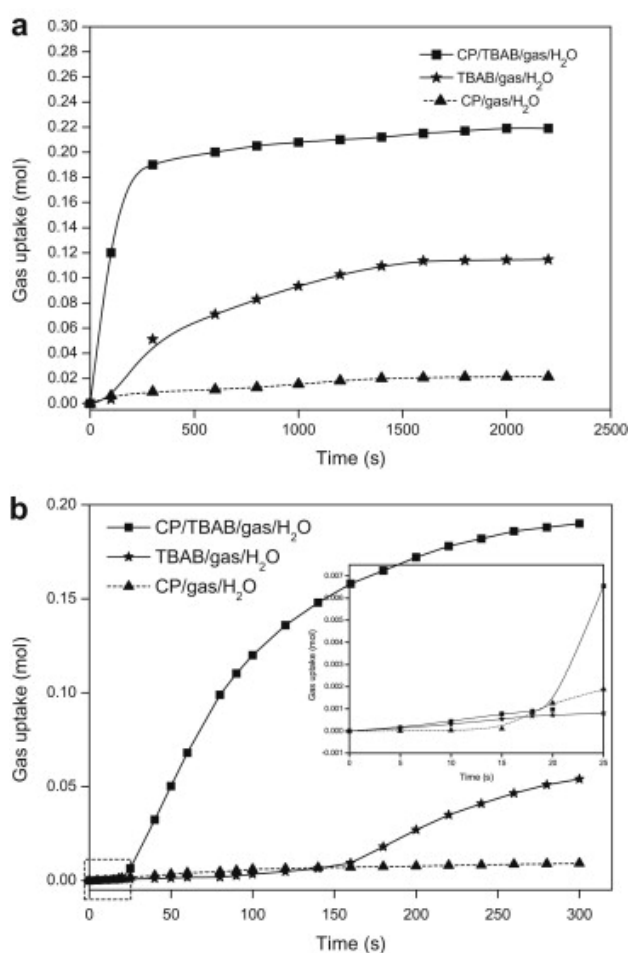


**Figure 2.24** Gas uptake change for hydrate formation vs. time from different systems at 276.15 K and 4.0 MPa (Li *et al.* 2012a).



## **CHAPTER III**

### **EXPERIMENTAL**

#### **3.1 Materials and Equipment**

##### 3.1.1 Materials

- Tetra-n-butylphosphonium bromide (TBPB, 99% purity from Alfa Aesar, United Kingdom)
- Tetra-n-butylammonium bromide (TBAB, 98% purity from Alfa Aesar, United Kingdom)
- Cyclopentane (CP, 95% purity from Alfa Aesar, United Kingdom)
- Ultra high purity methane gas (99.99% purity from Linde Co., Ltd., Thailand)
- Deionized water

##### 3.1.2 Equipments

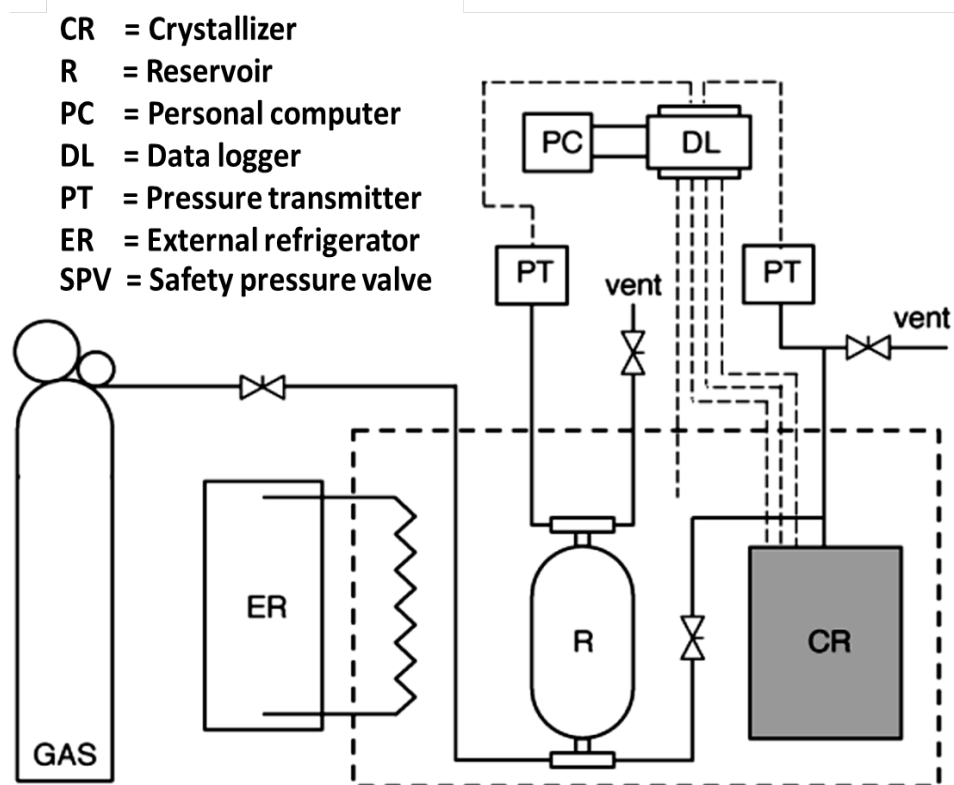
- Hydrate formation/dissociation apparatus
- Crystallizer (CR)
- Reservoir (R)
- Personal Computer (PC)
- Pressure transducer (PT)
- K-type thermocouple
- External Refrigerator (ER)

#### **3.2 Experimental Procedures**

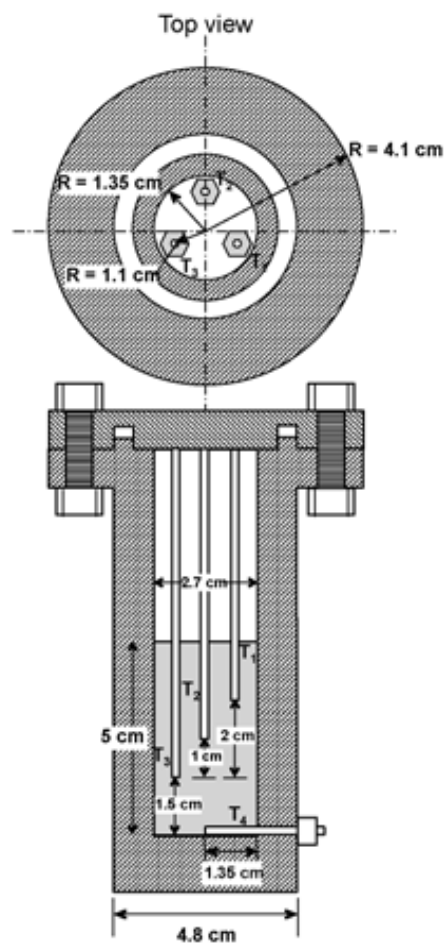
##### 3.2.1 Experimental Apparatus

Figure 3.1a shows the schematic of gas hydrate apparatus, which consisted of a reservoir (R), a high-pressure stainless steel crystallizer (CR), and the crystallizer. The reservoir was immersed in a cooling bath, the temperature of which was adjusted and controlled by an external controllable circulator. Two pressure

transmitters were used to measure the pressure. The temperature in the crystallizer was measured by four k-type thermocouples. Figure 5.1b illustrates cross-section of a crystallizer and the thermocouples at different positions in the reactor: T1 at the top of the bed, T2 at the middle of the bed, T3 at the bottom of the bed, and T4 at the bottom of the crystallizer. The data during the experiment were recorded by A data logger (AI210 Model, Wisco Industrial instruments, Thailand) connected to a computer. All experiments were carried out in the quiescent condition with a fixed amount gas and water in the closed system.



**Figure 3.1** Schematic of the experimental apparatus (Siangsai *et al.*, 2015).



**Figure 3.2** Cross-section of a crystallizer (Siangsai *et al.*, 2015).

### 3.2.2 Methane Hydrate Formation

The experimental procedure for the hydrate formation in the presence of 0 and 2.56 mol% of tetrabutylphosphonium bromide (TBPB), 0 and 2.56 mol% of tetraammonium bromide (TBAB), and 0, 5, 10, 15, and 20 %v/v cyclopentane (CP). After that methane gas was injected into the crystallizer through the valve of the gas supply at the desired experimental condition. The data was then recorded every 10 seconds. All hydrate formation experiments were carried out in the quiescent condition with a fixed amount of water and gas in the closed system. During the hydrate formation, the pressure in the crystallizer was decreased due to the gas consumption. The experiments continued until no significantly change in the

pressure. The pressure and temperature data is used to calculate for the methane consumption (gas uptake) using following Equation 3.1 (Siangsai *et al.*, 2015).

$$\Delta n_{H,t} = n_{H,0} - n_{H,t} = \left(\frac{PV}{zRT}\right)_{G,0} - \left(\frac{PV}{zRT}\right)_{G,t} \quad (3.1)$$

Where  $\Delta n_{H,t}$  = moles of consumed gas for hydrate formation, mol

$n_{H,t}$  = moles of hydrate at time  $t$ , mol

$n_{H,0}$  = moles of hydrate at time 0, mol

$P$  = pressure of the crystallizer, atm

$T$  = temperature of the crystallizer, K

$V$  = the volume of gas phase in the crystallizer,  $\text{cm}^3$

$Z$  = compressibility factor

$R$  =  $82.06 \text{ cm}^3 \cdot \text{atm} / \text{mol} \cdot \text{K}$

Subscripts of G,0 and G,t represent the gas phase at time zero and time  $t$  respectively. The methane hydrate yield was measured by Equation 3.2 in the closed system.

$$\text{Methane hydrate yield (mol\%)} = \frac{\text{Methane consumed (mol)}}{\text{Methane input (mol)}} \times 100 \quad (3.2)$$

### 3.2.3 Methane Hydrate Dissociation

After completion of methane hydrate formation, the methane hydrated was dissociated by thermal stimulation. The pressure in crystallizer was reduced carefully to the desired pressure by venting out the free gas in the system. Then, the temperature was increased from the formation temperature at the same heating rate for all experiments to the desired dissociation temperature. This point was marked as time zero for the dissociation experiment. The total moles of gas in the system equaled to the moles of gas at time zero. At any given time, the total number of moles ( $n_{T,t}$ ) in the system remains constant and equal to that at time zero ( $n_{T,0}$ ). Therefore, the mole of released methane from the hydrate at any time during the hydrate dissociation was calculated by Equation (3.2) (Siangsai *et al.*, 2015).

$$\Delta n_{H,\uparrow} = n_{H,t} - n_{H,0} = \left(\frac{PV}{zRT}\right)_{G,t} - \left(\frac{PV}{zRT}\right)_{G,0} \quad (3.3)$$

Where  $\Delta n_{H,\uparrow}$  = moles of released gas from the hydrate, mol

$n_{H,t}$  = moles of hydrate at time  $t$ , mol

$n_{H,0}$  = moles of hydrate at time 0, mol

$P$  = pressure of the crystallizer, atm

$T$  = temperature of the crystallizer, K

$V$  = the volume of gas phase in the crystallizer,  $\text{cm}^3$

$Z$  = compressibility factor

$R$  =  $82.06 \text{ cm}^3 \cdot \text{atm} / \text{mol} \cdot \text{K}$

Subscripts of G,0 and G,t represent the gas phase at time zero and time  $t$  respectively.

The percentage of methane recovery was calculated by Equation 3.4 (Siangsai *et al.*, 2015).

$$\% \text{Methane recovery} = \frac{(\Delta n_{H,\uparrow})_t}{(\Delta n_{H,\downarrow})_{t_{\text{end}}}} \times 100 \quad (3.4)$$

Where  $(\Delta n_{H,\uparrow})_t$  = moles of released gas from the hydrate during the hydrate dissociation at any given time, mol

$(\Delta n_{H,\downarrow})_{t_{\text{end}}}$  = moles of consumed gas for hydrate formation at the end of experiment, mol

## CHAPTER IV

### RESULTS AND DISCUSSION

This work, tetrabutylphosphonium bromide (TBPB), tetra-n-butyl ammonium bromide (TBAB) and cyclopentane (CP) were used as promoters to enhance methane hydrate formation at 2.5 °C and 8 MPa. Gas hydrate formation is an exothermic reaction so it can be noticed by an increase in the temperature with the increase in the gas uptake. After methane hydrate formation, the methane hydrate was dissociated by thermal stimulation starting at 7 MPa and temperature was increased to 25 °C.

#### 4.1 Effects of Tetrabutylphosphonium Bromide (TBPB)

Figure 4.1 provides information concerning experimental conditions for methane hydrate formation with TBPB solution at 2.5 °C and 8 MPa. The temperature and pressure profiles during the experiment are relatively constant.

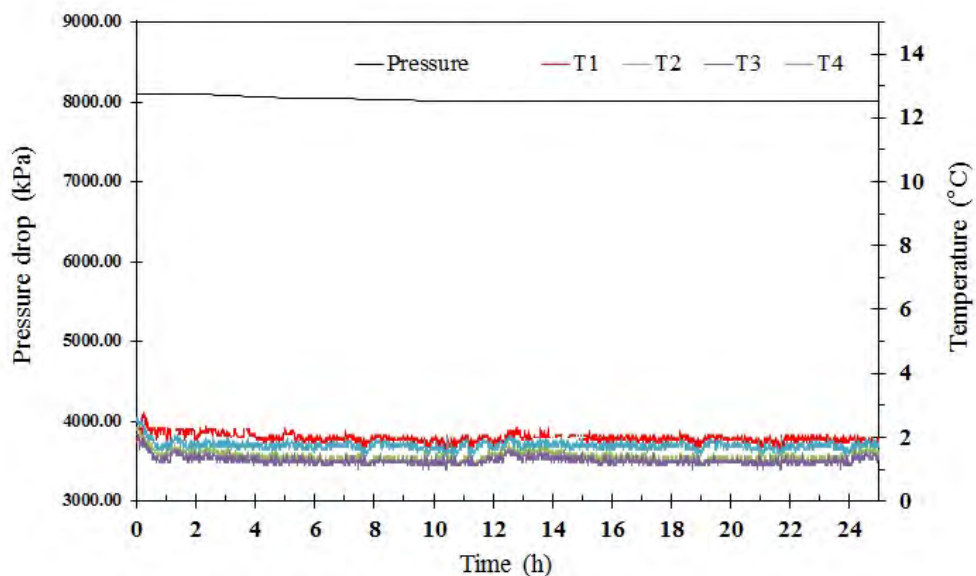


**Figure 4.1** Gas uptake and temperature profiles of the system with CH<sub>4</sub>, H<sub>2</sub>O, and 2.56 mol% TBAB forming at 2.5 °C and 8 MPa in the batch operation.

The result from figure 4.1 clearly indicates that 2.56 mol% TBPB does not show the evidence of methane hydrate formation. This result remains the same after 24 hours. It can be concluded that, in the quiescent close system, the presence of TBPB alone was not sufficient to promote methane hydrate formation. In general, the use of TBPB can enhance the semihydrate formation in the stirred tank reactor as reported by Iino *et al.* (2014) and Du *et al.* (2015). Stirring is an important technique that can enhance heat and mass transfer, and thus accelerating the speed of hydrate formation, while the heat transfer becomes a serious limitation to the application of quiescent reactor as the result in this work.

#### **4.2 Effects of Tetra-n-butyl Ammonium Bromide (TBAB)**

Table 4.1 provides information concerning experimental conditions for methane hydrate formation with TBAB solution at 2.5 °C and 8 MPa. The data show that the experiment conducted with pure water does not show the evidence of methane hydrate formation after 48 hours, while the hydrates form in the 2.56 mol% TBAB solution. The induction time in Table 4.1 confirms that the methane hydrate formation in the presence of 2.56 mol% TBAB occurs around 0.34 hours. Figure 4.2 shows that the temperature T2 is the highest temperature because the hydrate starts to form at the center of the crystallizer. It can be noted that the amount of the hydrates is significantly higher at the center than the other positions. However, the small amount of methane uptake ( $0.057 \pm 0.0011$  mol/mol of H<sub>2</sub>O) is due to gas dissolution into the solution. These results may be due to the fact that the methane hydrates form semihydrate structures, which take place rapidly and agglomerate at the high TBAB concentration. As reported by Li *et al.* (2010), the extensive hydrate formation and crystal agglomeration can block the methane gas that is coming into contact with water. This situation [leads to](#) poor gas storage capacity.

**Table 4.1** Experimental conditions for methane hydrate formation with TBAB at 2.5 °C and 8 MPa

Exp. No.	TBAB (mol%)	Induction time*(min)	Methane uptake (mol/mol of H <sub>2</sub> O)	Methane hydrate yield(mol%)
0	Pure water	NHF	-	-
1	2.56	31.80	0.0061	2.38
2	2.56	13.80	0.0046	1.81
3	2.56	21.00	0.0066	2.67
	<b>Avg.</b>	<b>22.20±9.06</b>	<b>0.057±0.001</b>	<b>2.29±0.44</b>

\*NHF is no hydrate formation.

\*Induction time is the time for the first hydrate formation.

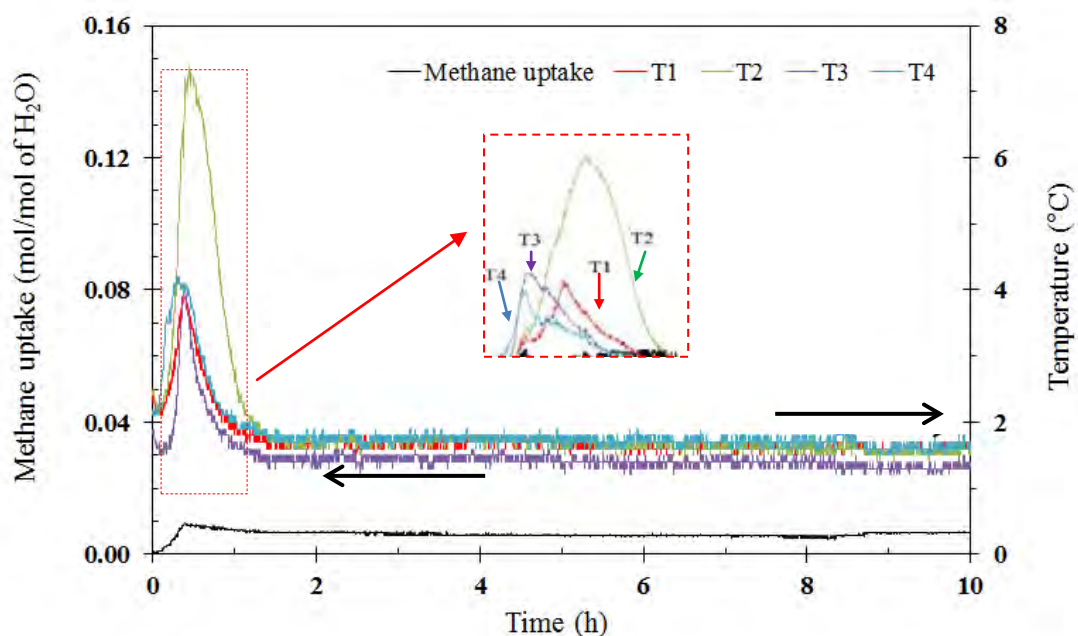


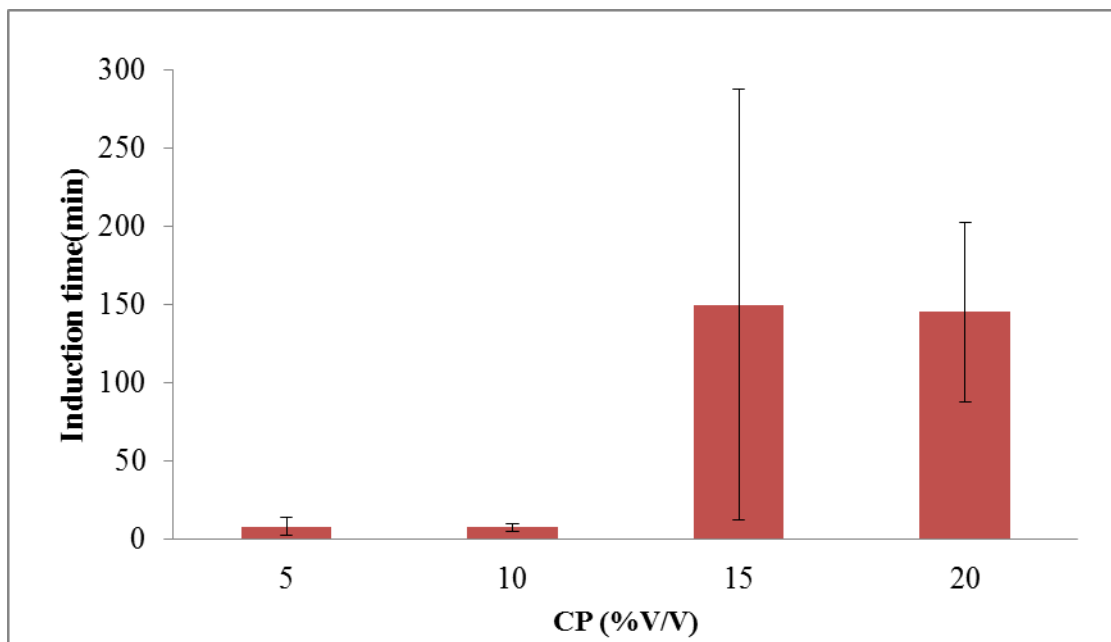
**Figure 4.2** Gas uptake and temperature profiles of forming TBAB hydrate at 2.5 °C and 8 MPa in batch operation (in the presence of 2.56 mol% TBAB) (Experiment 2).



### 4.3 Effects of Cyclopentane (CP)

#### 4.3.1 Effects of CP concentration

Experimental conditions of the methane hydrate formation in the presence of 5, 10, 15, and 20 %v/v is shown in Table 4.2. The induction time in the table indicates the time for the first hydrate formation. The effects of CP concentrations on the induction time are shown in Figure 4.3. As seen from the figure, the induction time increases with the increase in the concentration of CP. It may be noted that, the presence of different amounts of CP results in the different thickness of the CP layer in the unstirred reactor. As CP is immiscible and has lower density than water, it forms a clear layer above water. A larger amount of CP will result in a larger thickness of the CP layer, which can potentially increase the diffusion time required for the gas to come in contact with water for hydrate formation (Ho *et al.*, 2015).



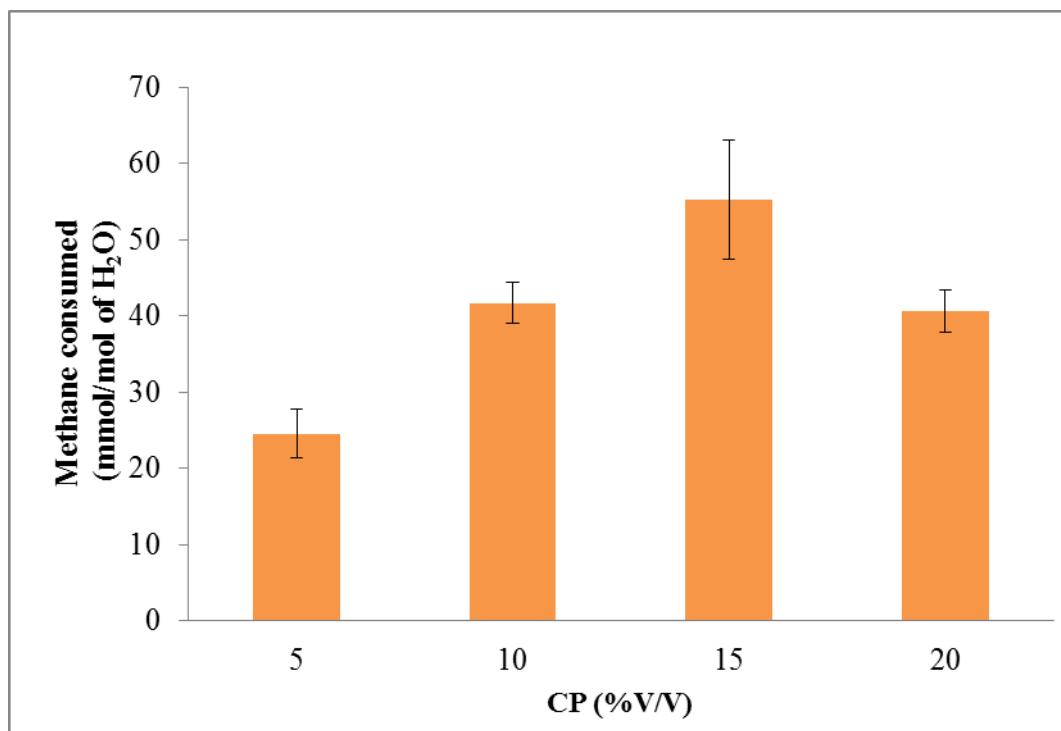
**Figure 4.3** Effects of CP concentrations (%V/V) on induction time of hydrate formation with CP at 2.5 °C and 8 MPa in the batch operation.

Figure 4.4 shows the effects of CP concentrations on methane consumed. As seen from the figure, the average methane consumption increases with the increase in the CP concentration. However, it decreases with increasing the amount of CP higher than 15 %v/v. Again, the CP layer may prevent gas from entering the hydrate phase as the experiment proceeds (Lv *et al.*, 2015).

**Table 4.2** Experimental conditions for methane hydrate formation with CP at 2.5 °C and 8 MPa

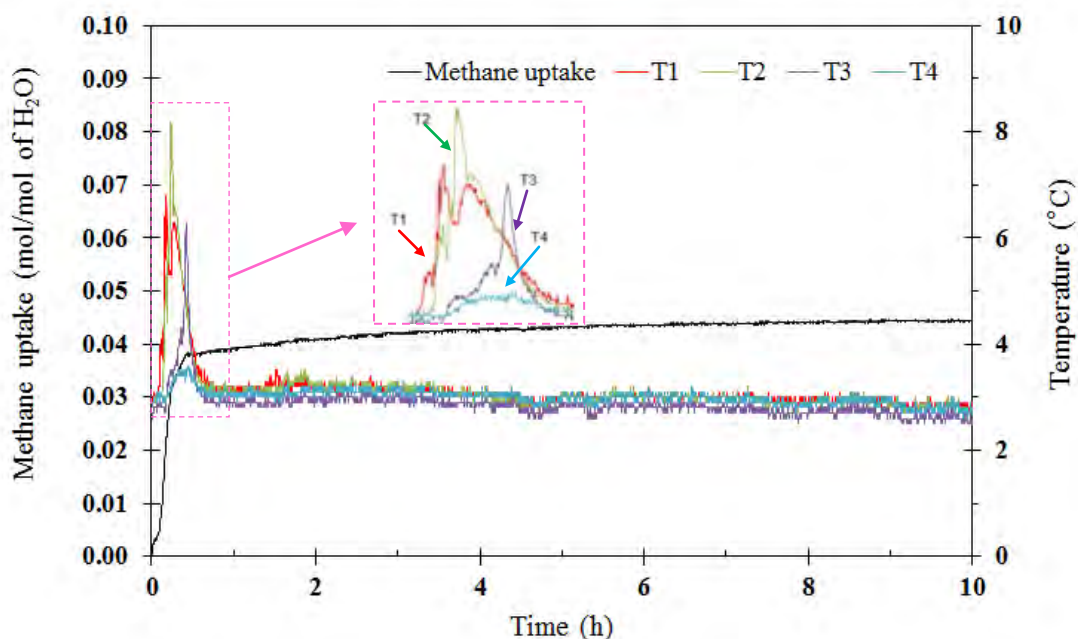
Exp. No.	CP (% V/V)	Induction time* (min)	Methane uptake (mol/mol of H <sub>2</sub> O)	Methane hydrate yield (mol%)
4	5	5.00	0.0216	12.09
5	5	15.00	0.0242	13.72
6	5	4.80	0.0279	15.85
	<b>Avg.</b>	<b>8.27±5.83</b>	<b>0.0246±0.0031</b>	<b>13.89±1.89</b>
7	10	4.80	0.0446	24.19
8	10	9.60	0.0413	21.16
9	10	9.00	0.0392	20.06
	<b>Avg.</b>	<b>7.80±2.62</b>	<b>0.0417±0.0027</b>	<b>21.80±2.14</b>
10	15	30.00	0.0628	31.99
11	15	300.00	0.0472	22.95
12	15	120.00	0.0557	28.38
	<b>Avg.</b>	<b>150.00±137.48</b>	<b>0.0552±0.0078</b>	<b>27.77±4.55</b>
13	20	126.00	0.0438	20.22
14	20	100.02	0.0395	18.47
15	20	210.00	0.0386	17.79
	<b>Avg.</b>	<b>145.34±57.48</b>	<b>0.0406±0.0027</b>	<b>18.83±1.25</b>

\*Induction time is the time for the first hydrate formation.



**Figure 4.4** Effects of CP concentrations (% V/V) on methane consumed of hydrate formation with CP at 2.5 °C and 8 MPa in the batch operation.

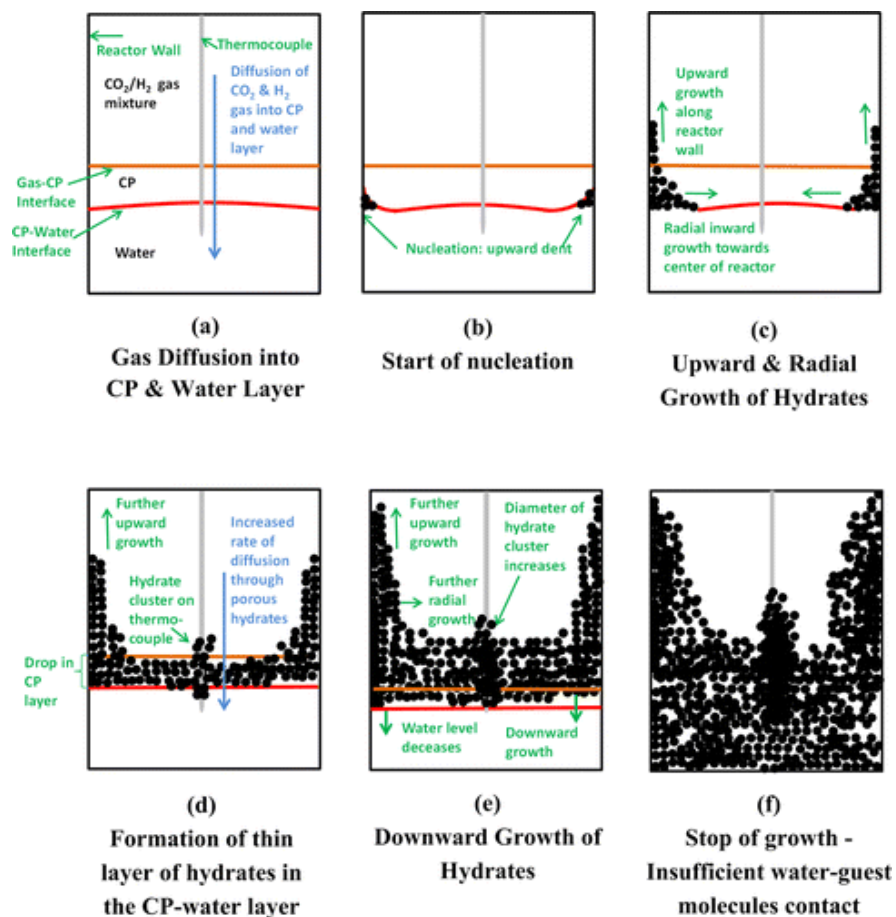
Figure 4.5 shows typical methane hydrate formation experiments with 10 %V/V CP solution at 2.5 °C. The temperature profiles in the crystallizer, recorded by the four thermocouples (different position), indicate that the temperature in the crystallizer rises at T1 first followed by T2, T3, and T4, before the gas uptake increases rapidly. It can be deduced that the hydrates form from the top to the bottom of the crystallizer. Lim *et al.* (2013) proposed the mechanism of methane hydrate formation that the nucleation occurred at the CP-water interface. The hydrate fronts grow upward along the crystallizer walls and radially inward toward the center of the crystallizer. Finally, the bottom layer was fully filled with hydrates while, in the top gas phase layer, the amount of hydrates filled up was lower, as shown in Figure 4.6.



**Figure 4.5** Typical methane consumption and temperature profiles during the methane hydrate formation experiments performed with 10 %V/V at 2.5 °C (Experiment 7, Table 4.2).

Figure 4.6 shows the gas uptake and temperature profiles of hydrate formation with 10 %V/V and 15 %V/V of CP solution. First, the amount of gas uptake increases because of dissolution methane in water until it saturates. After that, the rate of gas uptake suddenly increases due to methane hydrate formation. The start of hydrate formation experiment can be observed with the increased temperature profiles in the system (exothermic process). As seen from the figure, the experiment conducted with 15 %V/V of CP solution takes longer time to form hydrates than that with 10 %V/V of CP solution. The results show that the amount of methane uptake of 15 %V/V is higher than 10 %V/V of CP solution. Lv *et al.* (2015) reported that CP mainly occupies the large cavities ( $5^{12}6^4$ ), and methane is encapsulated in the small cavities ( $5^{12}$ ) of the structure II hydrates. With the increase in the volume of CP in the liquid phase, the more CP molecules make an entrance into the large cavities of the SII, hydrates and the stabilization effect on hydrate formation is higher with the increase of the volume of CP in the liquid phase. However, the excess CP

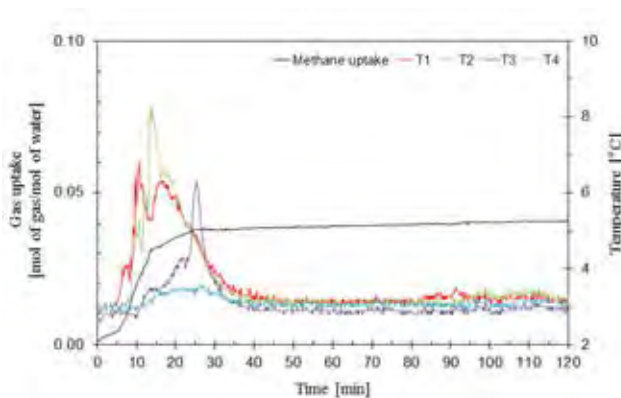
molecules lead to the decrease in the structure II hydrate formation and gas diffusion due to the decrease in the volume of water.



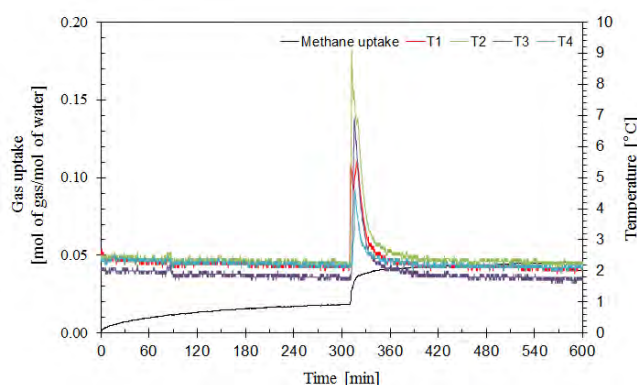
**Figure 4.6** Pictorial illustration of the mechanism of  $\text{CO}_2\text{-H}_2\text{-CP}$  hydrates in an unstirred system (Lim *et al.*, 2015).

Figure 4.8 presents the effects of CP concentrations on methane hydrate yield, which can be considered as a value to enrich the methane storage in the hydrate form. Methane hydrate yield is important for methane hydrate storage and transport applications for methane gas production after storing methane gas in the hydrate formation. As seen from the figure, 15 %V/V CP shows the highest average methane hydrate yield at about 27.77 mol% followed by 10 %V/V, 20 %V/V, and 5 %V/V of CP, respectively. Based on these results, the methane hydrate yield of 10 %V/V and 20 %V/V CP is about the same, while 15 %V/V CP

is significantly higher. It can be noted that there may be an optimum concentration of the hydrate formation promoter. Lim *et al.* (2013) reported that the superior performance of unstirred reactor over stirred reactor in hydrate based gas separation process (HBGS) for carbon dioxide capture was due to the presence of immiscible CP layer above the water. The CP layer aided in diffusion of guest gas to the bulk phase in an unstirred reactor, while in stirred reactor, CP was dispersed in bulk phase due to stirring. Furthermore, advantages of employing CP and an unstirred reactor configuration are both capital costs (compression costs) and operating costs (Ho *et al.*, 2015). However, not only methane hydrate yield but also methane dissociation is required for methane gas after storing methane gas utilization for methane storage and transport applications.



(a)



(b)

**Figure 4.7** Typical methane consumption and temperature profiles during the methane hydrate formation experiments performed with CP at 2.5 °C: (a) 10 % V/V (Experiment 7, Table 4.2), (b) 15 % V/V (Experiment 11, Table 4.2).

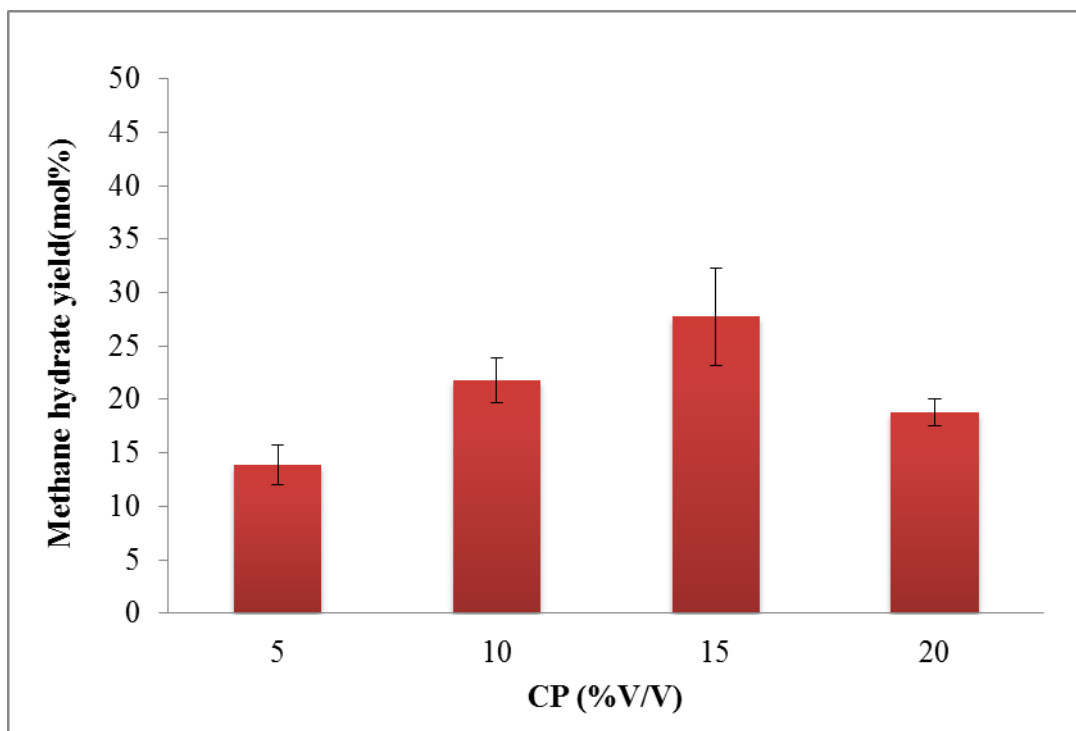


**Figure 4.8** Effects of CP concentrations (%V/V) on methane hydrate yield on methane consumed of hydrate formation with CP at 2.5 °C and 8 MPa in the batch operation.

#### 4.3.2 Effects of Temperature

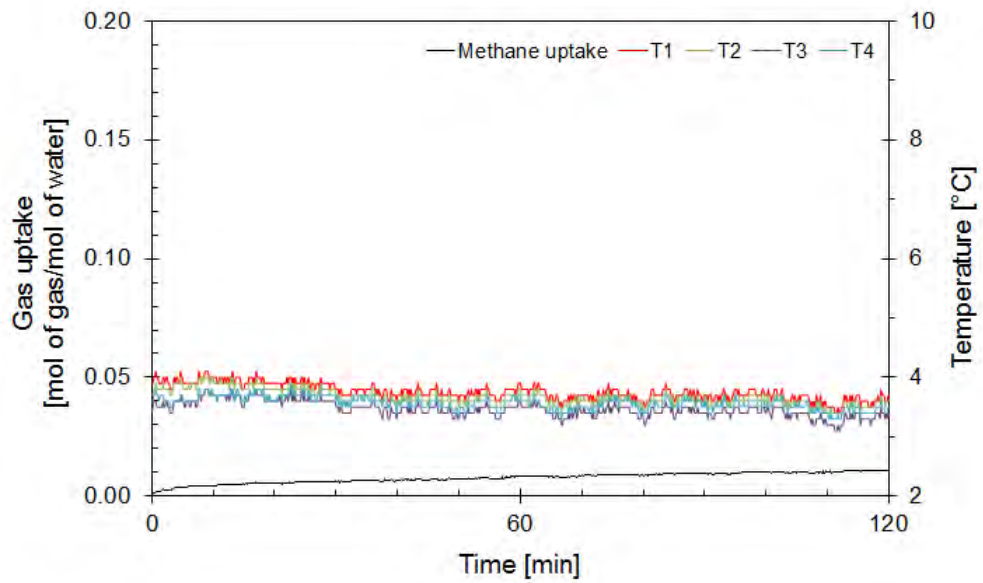
Figure 4.9 provides information concerning experimental conditions for methane hydrate formation with 15 %v/v CP at 4 °C and 8 MPa. The temperature and pressure profiles during the experiment are relatively constant. The figure clearly indicates that 15 %v/v CP does not show the evidence of methane hydrate formation at 4 °C, while 15 %v/v CP the hydrates form at 2.5 °C. These results may be due to the decrease in the formation temperature (from 4 °C to 2.5 °C) increases the gas diffusion into the CP layer, which results in the ease in the hydrate formation. However, the presence of 10 %v/v CP at 4 °C was sufficient to promote methane hydrate formation as summarized in Table 4.3. A *comparison between the results* of methane hydrate formation at 4 °C and 2.5 °C indicates that the total moles of gas consumed increases with the decreases in the experimental temperature, and the

average methane hydrate yield also increases by two folds. The average gas consumption increases from 0.03 mol/mol of H<sub>2</sub>O to 0.04 mol/mol of H<sub>2</sub>O due to the decreases in the formation temperature from 4 °C to 2.5 °C. This result is consistent with a report by Lim *et al.* (2013), who reported that the total mole of gas consumed increased with the increase in the driving force. The increase in the amount of the gas going into the solution correlates with the enhancement of the gas hydrate growth rate, which also means the enhancement of the gas consumption rate.

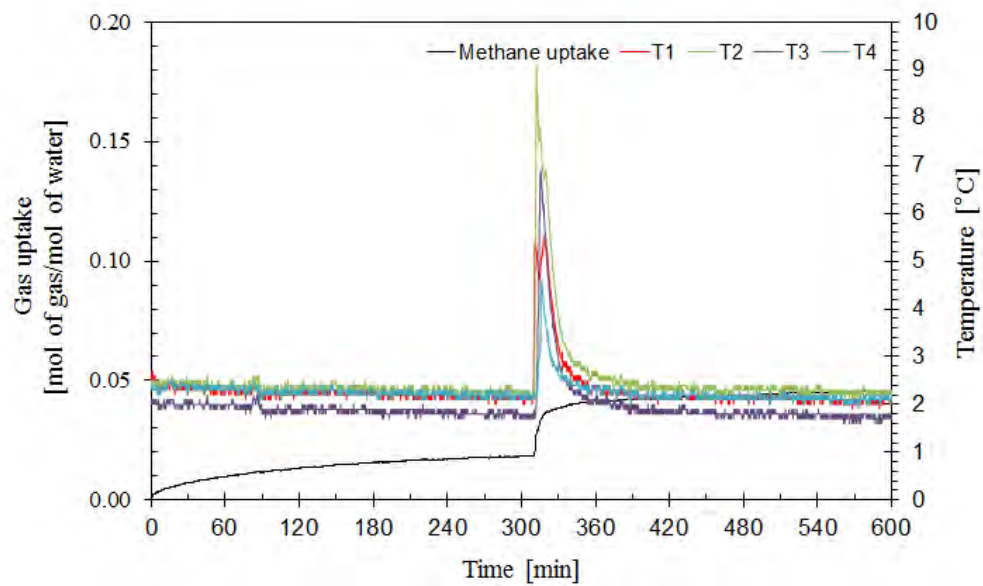
**Table 4.3** Experimental conditions for methane hydrate formation with 10 %V/V of CP at 2.5 °C and 4 °C (8MPa)

Exp. No.	Experimental temperature (°C)	Induction time (min)	Methane consumed (mol/mol of H <sub>2</sub> O)	Methane hydrate yield (mol%)
<b>7</b>	2.5	4.80	0.0446	24.19
<b>8</b>	2.5	9.60	0.0413	21.16
<b>9</b>	2.5	9.00	0.0392	20.06
	<b>Avg.</b>	<b>7.80±2.62</b>	<b>0.0417±0.0027</b>	<b>21.80±2.14</b>
<b>16</b>	4	10.20	0.0367	11.17
<b>17</b>	4	9.00	0.0336	10.32
<b>18</b>	4	10.80	0.0344	10.41
	<b>Avg.</b>	<b>10.00±0.92</b>	<b>0.0349±0.0016</b>	<b>10.63±0.47</b>





(a)



(b)

**Figure 4.9** Typical methane consumption and temperature profiles during the methane hydrate formation experiments performed with CP at 8 Mpa: (a) 15 % V/V CP at 4 °C, (b) 15 % V/V CP at 2.5 °C (Experiment 11, Table 4.2).

### 4.3.3 Methane Hydrate Dissociation

After the hydrate formation was complete, the methane hydrates were dissociated by thermal stimulation method. The temperatures in the crystallizer were increased from the formation temperature at the same heating rate for all experiments to the set point (25 °C). Figure 4.10 shows the experimental conditions for methane hydrate dissociation with various CP concentrations at 25 °C. The experiment number in the table corresponds to the methane hydrate formation experimental conditions in Table 4.2. The temperature from each thermocouple gradually increases with the water temperature. Methane starts to release around 4.5 °C, which can be observed by the change of the temperature profiles in the crystallizer (T1, T2, T3, and T4). As seen from the figure, the temperature of the thermocouples in the crystallizer is lower than the water temperature during the dissociation process due to endothermic reaction. Finally, all temperatures become the same again after the dissociation completes.

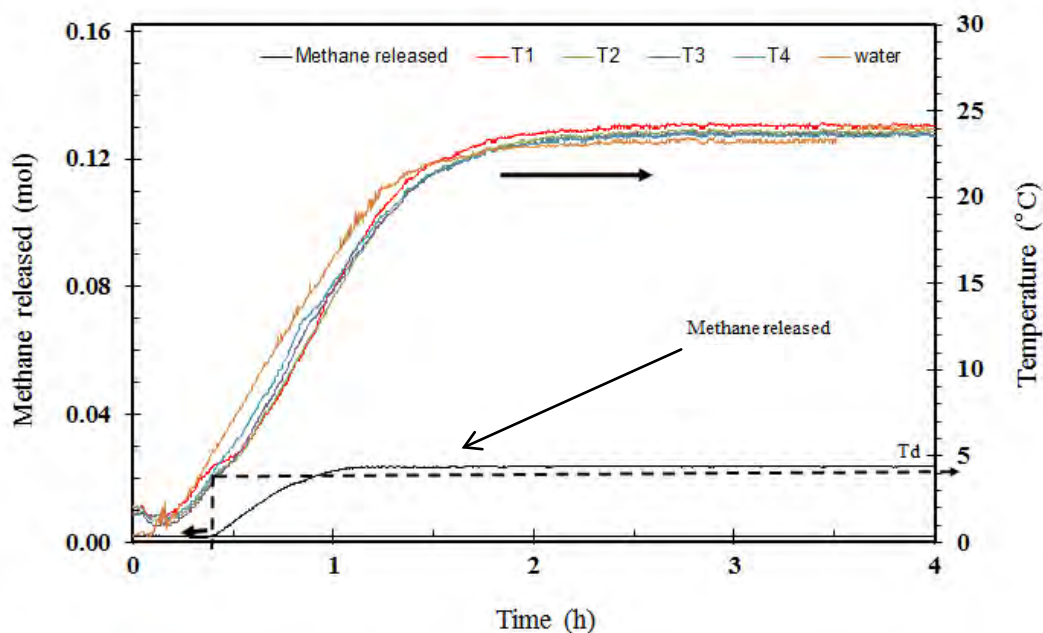


**Figure 4.10** Typical methane released and temperature profiles during methane hydrate dissociation with the presence of 15 %V/V of CP (Experiment 10, Table 4.3).

**Table 4.4** Experimental conditions for methane hydrate dissociation in presence of CP at various % V/V

Exp. No.	CP (% V/V)	Dissociation temperature $T_d^*$ (°C)	Driving force temperature $**$ (°C)
4	5	10	7.5
5	5	13	10.5
6	5	6	3.5
	<b>Avg.</b>	<b>9.7±3.5</b>	<b>7.2±3.5</b>
7	10	11	8.5
8	10	9.5	7
9	10	9.5	7
	<b>Avg.</b>	<b>10.0±0.9</b>	<b>7.5±0.9</b>
10	15	4.5	2
11	15	8	5.5
12	15	9	6.5
	<b>Avg.</b>	<b>7.2±2.4</b>	<b>4.7±2.4</b>
13	20	9.5	7
14	20	10	7.5
15	20	13	10.5
	<b>Avg.</b>	<b>10.8±1.9</b>	<b>8.3±1.9</b>

\* $T_d$  is the dissociation temperature at which methane released for the initial pressure.

\*\*Driving force temperature is the different temperature between the experimental temperature and the dissociation temperature.

**Table 4.5** Methane released and methane recovery in presence of CP at various %V/V

Exp. No.	CP (% V/V)	Methane released (mol)	Methane recovery (mol%)
4	5	0.0013	5.84
5	5	0.0038	15.50
6	5	0.0017	5.96
	<b>Avg.</b>	<b>0.0022± 0.0013</b>	<b>9.10± 5.54</b>
7	10	0.0053	11.79
8	10	0.0050	12.13
9	10	0.0100	25.51
	<b>Avg.</b>	<b>0.0068±0.0028</b>	<b>16.47±7.82</b>
10	15	0.0217	34.49
11	15	0.0105	22.17
12	15	0.0086	15.53
	<b>Avg.</b>	<b>0.0136±0.0071</b>	<b>24.06±9.62</b>
13	20	0.0009	2.14
14	20	0.0011	2.77
15	20	0.0002	0.56
	<b>Avg.</b>	<b>0.0007±0.0005</b>	<b>1.82±1.14</b>

Table 4.4 shows the experimental conditions for methane hydrate dissociation with various %V/V CP. The data are divided into two parts, namely dissociation temperature, and driving force temperature. The driving force temperature is the different temperature between the experimental temperature and the dissociation temperature. It can be seen that, the experiments conducted with 15 %V/V of CP has the lowest driving force temperature. The highest methane recovery is from the experiments conducted with 15 %V/V CP, amounting to

24.06%, as shown in Table 4.5. Based on the results, it can be concluded that 15 %V/V of CP is the optimal concentration for 2.5 °C and 8 MPa conditions.

Furthermore, the driving force temperature influences the rate of methane released during methane hydrate dissociation. At higher driving force temperature, the hydrates dissociate slower than that at lower driving force temperature. It can be noted that the driving force temperature indicates the stability zone, which is the period between the experimental point and the dissociation point (Siangsai *et al.*, 2015).

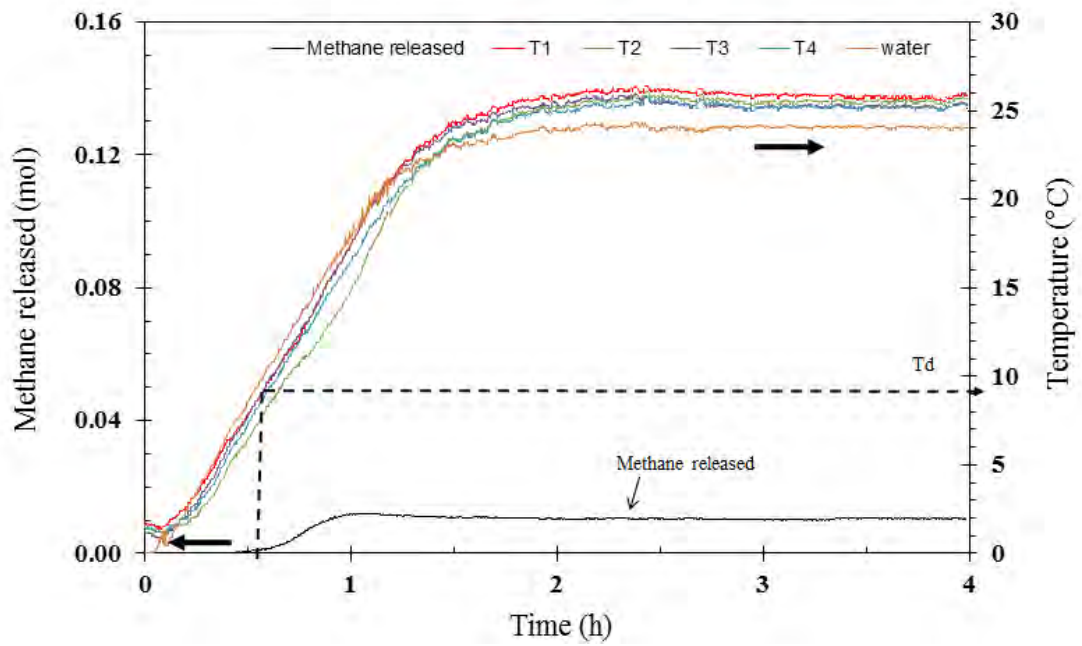
Figure 4.11a and Figure 4.11b indicate that the experiments conducted at 2.5 °C and 4 °C, respectively. It can be seen that, at the same 10 %V/V of CP. As seen from table 4.6 and figure 4.11, it can be observed that the driving force temperature increases with the decrease in the temperature. Therefore, the experiment conducted at lower temperature has more hydrate stability than that at higher temperature. However, the experiment conducted at 4 °C has a higher methane recovery than that the experiment conducted at 2.5 °C, as seen in Table 4.6.

**Table 4.6** Experimental conditions for methane hydrate formation with 10 %V/V of CP at 2.5 °C and 4 °C (8MPa)

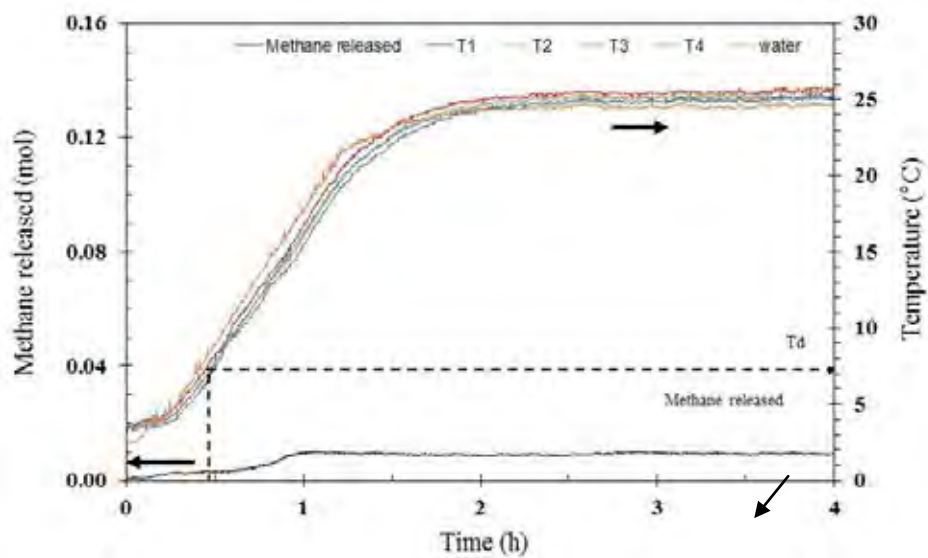
Exp. No.	Exp. temperature (°C)	Dissociation temperature, $T_d$ (°C)	Driving force temperature (°C)	Methane released (mol)	Methane recovery (mol%)
<b>7</b>	2.5	11	8.5	0.0053	11.79
<b>8</b>	2.5	9.5	7	0.0050	12.13
<b>9</b>	2.5	9.5	7	0.0100	25.51
	<b>Avg.</b>	<b>10.0±0.9</b>	<b>7.5±0.9</b>	<b>0.0068±0.0028</b>	<b>16.47±7.82</b>
<b>16</b>	4	7	3	0.0074	20.12
<b>17</b>	4	8	4	0.0060	17.91
<b>18</b>	4	8	4	0.0090	26.15
	<b>Avg.</b>	<b>8.0±0.6</b>	<b>4.0±0.6</b>	<b>0.0075±0.0015</b>	<b>21.40±4.26</b>

\* $T_d$  is the dissociation temperature at which methane released for the initial pressure.

\*\*Driving force temperature is the different temperature between the experimental temperature and the dissociation temperature.



(a)



(b)

**Figure 4.11** Typical methane released and temperature profiles during methane hydrate dissociation with the presence of 10 % V/V CP: (a) 2.5 °C (Experiment 8, Table 4.6), (b) 4 °C (Experiment 16, Table 4.6).

## **CHAPTER V**

### **CONCLUSIONS AND RECOMMENDATIONS**

#### **5.1 Conclusions**

In this work, methane hydrate formation and dissociation in the presence of different cyclopentane (CP), tetra-n-butyl phosphonium bromide (TBPB) and tetra-n-butyl ammonium bromide (TBAB) concentrations were investigated. The results showed that the addition of TBAB and CP shortened the induction time. The presence of TBPB alone was not sufficient to promote methane hydrate formation. The addition of TBAB promoted methane hydrate formation with only insignificant methane uptake. In the presence of CP, the induction time increased with the increase in the concentration of CP due to the different thickness of the CP layer in the unstirred reactor. The average methane consumption increased with the increase in the concentration of CP. 15 %V/V of CP was the optimal concentration for 2.5 °C and 8 MPa conditions giving the highest average methane consumption and methane hydrate yield. The average gas consumption and methane hydrate yield increased with the decrease in the experimental temperature. For methane hydrate dissociation, the driving force temperature increased with the decrease in the temperature. The experiment conducted at lower temperature had more hydrate stability than that at higher temperature.

#### **5.2 Recommendations**

To observe the mechanism of gas hydrate formation, the gas hydrate apparatus should be redesigned. The crystallizer with observation window should be applied in the crystallizer.

## REFERENCES

- Aliabadi, M., Rasoolzadeh, A., Esmailzadeh, F., and Alamdari, A. (2015) Experimental study of using CuO nanoparticles as a methane hydrate promoter. Journal of Natural Gas Science and Engineering, 27, 1518-1522.
- Archer, D. (2007) Methane hydrate stability and anthropogenic climate change. Biogeosciences, 4, 521-544.
- Asheesh, K., Gaurav, B., Kulkarni, B. D., and Rajnish, K. (2014) Role of surfactants in promoting gas hydrate formation. Industrial and Engineering Chemistry Research, 54 (49), 12217-12232.
- Babakhani, S. and Alamdari, A. (2015) Effect of maize starch on methane hydrate formation/dissociation rates and stability. Journal of Natural Gas Science and Engineering, 26, 1-5.
- Cai, J., Xu, C.G., Lin, F.H., Yu, H.Z., and Li, X.S. (2016) A novel method for evaluating effects of promoters on hydrate formation. Energy, 102, 567-575.
- Chong, Z.R., Yang, S.B., Babu, P., Linga, P., and Li, X.S. (2016) Review of natural gas hydrates as an energy resource: Prospects and challenges. Applied Energy, 162, 1633-1652.
- Demirbas, A. (2010) Methane Gas Hydrate. New York: Springer.
- Deschamps, J. and Dalmazzone, D. (2010) Hydrogen storage in semiclathrate Hydrates of tetrabutyl ammonium chloride and tetrabutyl phosphonium bromide. Journal of Chemical and Engineering Data, 55(9), 3395-3399.
- Dou, B., Gao, H., Fan, B., and Ren, L. (2013) Modeling natural gas productivity recovery from a hydrate reservoir well. Journal of Natural Gas Science and Engineering, 5(4), 4-8.
- Du, J., Li, H., and Wang, L. (2014a) Effects of ionic surfactants on methane hydrate formation kinetics in a static system. Advanced Powder Technology, 25(4), 1227-1233.



- Du, J., Li, H., and Wang, L. (2014b) Phase equilibria and methane enrichment of clathrate hydrates of mine ventilation air + tetrabutylphosphonium bromide. Industrial and Engineering Chemistry Research, 53(19), 8182-8187.
- Du, J., Li, H. and Wang, L. (2015) Thermodynamic stability conditions, methane enrichment, and gas uptake of ionic clathrate hydrates of mine ventilation air. Chemical Engineering Journal, 273, 75-81.
- Duc, N. H., Chauvy, F., and Herri, J. M. (2007) CO<sub>2</sub> capture by hydrate crystallization—a potential solution for gas emission of steelmaking industry. Energy Conversion and Management, 48(4), 1313-1322.
- Godishala, K.K., Sangwai, J. S., Sami, N.A., and Das, K. (2013) Phase stability of semiclathrate hydrates of carbon dioxide in synthetic sea water. Journal of Chemical and Engineering Data, 58(4), 1062-1067.
- Grim, R. (2014) A Spectroscopic Study of the Structure and Occupancies of Clathrate Hydrates Incorporating Hydrogen. Ph.D. Thesis, Colorado School of Mines, Colorado, United states of America.
- Gudmundsson, J.S., Mork, M., and Graff, O.F. (2002) Hydrate non-pipeline technology. Proceedings of the fourth international conference on gas hydrate, 76, 997-1002.
- Ho, C. L., Babu, P., Kumar, R., and Linga P. (2015) HBGS (hydrate based gas separation) process for carbon dioxide capture employing an unstirred reactor with cyclopentane. Energy, 63, 252-259.
- Iino, K., Sakakibara, Y., Suginaka, T., and Ohmura, R. (2014) Phase equilibria for the ionic semiclathrate hydrate formed with tetrabutylphosphonium chloride plus CO<sub>2</sub>, CH<sub>4</sub>, or N<sub>2</sub>. The Journal of Chemical Thermodynamics, 71, 133-136.
- Jorge, F. and Gabitto, T. (2010) Review article physical properties of gas hydrates: A review. Journal of Thermodynamics, 80, 2010-2019.
- Kim, N.J., Lee J., Cho, Y., and Chun, W. (2010) Formation enhancement of methane hydrate for natural gas transport and storage. Energy, 35(6), 2717-2722.

- Kumar, A., Bhattacharjee, G., Kulkarni, B.D., and Kumar, R. (2015) Role of surfactants in promoting gas hydrate formation. Industrial and Engineering Chemistry Research, 54(49), 12217-12232.
- Li, D.L., Du, J.W., Fan, S.S., Liang, D.Q., Li, X.S., and Huang, N.S. (2007) Clathrate dissociation conditions for methane + tetra-n-butyl ammonium bromide (TBAB) + water. Journal of Chemical and Engineering Data, 52(5), 1916-1918.
- Li, X.S., Cai, J., Chen, Z.Y., and Xu, C.G. (2012a) Hydrate-based methane separation from the drainage coal-bed Methane with tetrahydrofuran solution in the presence of sodium dodecyl sulfate. Energy and Fuels, 26(2), 1144-1151.
- Li, X.S., Xu, C.G., Chen, Z.Y., and Cai J. (2012b) Synergic effect of cyclo-pentane and tetra-n-butyl ammonium bromide on hydrate-based carbon dioxide separation from fuel gas mixture by measurements of gas uptake and X-ray diffraction patterns. International Journal of Hydrogen Energy, 37(1), 720-727.
- Lim, Y.A., Babu P., Kumar R., and Linga P. (2013) Morphology of carbon dioxide–hydrogen–cyclopentane hydrates with or without sodium dodecyl sulfate. Crystal Growth and Design, 13 (5), 2047-2059.
- Lv, Q., Li, L., Li, X., and Chen, Z. (2015) Formation kinetics of cyclopentane + methane hydrates in brine water systems and raman spectroscopic analysis. Energy and Fuels, 29 (9), 6104-6110.
- Mech, D., Pandey, G., and Sangwai, J. S. (2015) Effect of NaCl, methanol and ethylene glycol on the phase equilibrium of methane hydrate in aqueous solutions of tetrahydrofuran (THF) and tetra-n-butyl ammonium bromide (TBAB). Fluid Phase Equilibria, 402, 9-17.
- Muromachi, S., Takeya, S., Yamamoto, Y., and Ohmura, R. (2014) Characterization of tetra-n-butylphosphonium bromide semiclathrate hydrate by crystal structure analysis. Crystal Engineering Communication, 16(10), 2056-2060.

- Ripmeester, J.A., Tse, J.S, Ratcliffe, C.I., and Powell, B.M. (1987) A new clathrate hydrate structure. Nature, 325, 135-136.
- Shi, L.L., Liang, D.Q. and Li, D.L. (2013) Phase equilibrium data of tetrabutylphosphonium bromide plus carbon dioxide or nitrogen semiclathrate hydrates. Journal of Chemical and Engineering Data, 58(7), 2125-2130.
- Siangsai, A., Rangsunvigit, P., Kitiyanan, B., and Kulprathipanja, S. (2015) Roles of activated carbon and tetrahydrofuran on methane hydrate phase equilibrium. Chemical Engineering Transactions, 39, 1195-1200.
- Sloan, E.D. (1998a) Gas Hydrates: Review of physical/chemical properties. Energy Fuels, 12(2), 191-196
- Sloan, E.D. Clathrate Hydrates of Natural Gases. (1998b) New York : Marcel Dekkar
- Suginaka, T., Sakamoto, H., Iino, K., Takeya, S., Nakajima, M., and Ohmura, R. (2012) Thermodynamic properties of ionic semiclathrate hydrate formed with tetrabutylphosphonium bromide. Fluid Phase Equilibria, 317, 25-28.
- Sun, Z.G. and Sun, L. (2010) Equilibrium conditions of semi-clathrate hydrate dissociation for methane + tetra-n-butyl ammonium bromide. Journal of Chemical and Engineering Data, 55(9), 3538-3541.
- Thomas, S. and Dawe, R.A. (2003) Review of ways to transport natural gas energy from countries which do not need the gas for domestic use. Energy, 28(14), 1461-1477.
- Veluswamy, H.P., Chen, J.Y., and Linga, P. (2015) Surfactant effect on the kinetics of mixed hydrogen/propane hydrate formation for hydrogen storage as clathrates. Chemical Engineering Science, 126, 488-499.
- Verrett, J., Posteraro, D., and Servio, P. (2012) Surfactant effects on methane solubility and mole fraction during hydrate growth. Chemical Engineering Science, 84, 80-84.
- Wang, F., Jia, Z.Z., Luo, S.J., Fu, S.F., Wang, L., Shi, X.S., and Guo, R.B. (2015) Effects of different anionic surfactants on methane hydrate formation. Chemical Engineering Science, 137, 896-903.

- Wang, X. and Dennis, M. (2015) An experimental study on the formation behavior of single and binary hydrates of TBAB, TBAF and TBPB for cold storage air conditioning applications. Chemical Engineering Science, 137, 938-946.
- Wang, X. and Dennis, M. (2016) Characterisation of thermal properties and charging performance of semi-clathrate hydrates for cold storage applications. Applied Energy, 167, 59-69.
- Winters, W.J., Pecher, I.A., and Waite, W.F. (2004) Physical properties and rock physics models of sediment containing natural and laboratory-formed methane gas hydrate. American Mineralogist, 89(8), 1221-1227.
- Ye, N. and Zhang, P. (2014) Phase equilibrium and morphology characteristics of hydrates formed by tetra-n-butyl ammonium chloride and tetra-n-butyl phosphonium chloride with and without CO<sub>2</sub>. Fluid Phase Equilibria, 361, 208-214
- Zarenezhad, B. and Varaminian, F. (2013) A unified approach for description of gas hydrate formation kinetics in the presence of kinetic promoters in gas hydrate converters. Energy Conversion and Management, 73, 144-149.
- Zheng, J., Yang, M., Liu, Y., Wang, D., and Song, Y. (2017) Effects of cyclo-pentane on CO<sub>2</sub> hydrate formation and dissociation as a co-guest molecule for desalination. The Journal of Chemical Thermodynamics, 104, 9-15.
- “Methane Hydrates” Energy Resource Potential of Methane Hydrate, 8 Nov 2013. 5 May 2015. < <http://www7430.nrlssc.navy.mil> >.
- “Methane Hydrates” Gas Craters Off Norway Linked to Fringe Bermuda Triangle Theory, 19 June 2012. 1 May 2015 < <http://www.news.nationalgeographic.com> >.
- “Tetra-n-butylphosphonium bromide (TBPB)” structure of TBPB, 5 May 2007. 1 Nov 2015 < <http://www.chemicalbook.com> >.

## APPENDICES

### Appendix A Calculation for the Methane Consumption

From; 
$$\Delta n_{H,t} = n_{H,0} - n_{H,t} = \left( \frac{PV}{zRT} \right)_{G,0} - \left( \frac{PV}{zRT} \right)_{G,t}$$

Where,  $\Delta n_{H,t}$  = moles of consumed gas for hydrate formation, mol

$n_{H,t}$  = moles of hydrate at time  $t$ , mol

$n_{H,0}$  = moles of hydrate at time 0, mol

$P$  = pressure of the crystallizer, atm

$T$  = temperature of the crystallizer, K

$V$  = the volume of gas phase in the crystallizer,  $\text{cm}^3$

$z$  = compressibility factor

$R$  =  $82.06 \text{ cm}^3 \cdot \text{atm} / \text{mol} \cdot \text{K}$

#### Properties of carbon dioxide

Critical Temperature ( $T_c$ ) = 190.45 K

Critical Pressure ( $P_c$ ) = 4596 kPa

Acentric Factor ( $\omega$ ) = 0.0115

#### Properties of additive

Density of tetra-n-butyl phosphonium bromide (TBPB) in pure water =  $1.039 \text{ g/cm}^3$

Molecular weight of TBPB = 339.342 g/mol

Purity of TBPB = 98%

Density of tetra-n-butyl ammonium bromide (TBAB) in pure water =  $1.039 \text{ g/cm}^3$

Molecular weight of TBAB = 322.38 g/mol

Purity of TBAB = 98%

Density of Cyclopentane (CP) in pure water =  $0.751 \text{ g/cm}^3$

Molecular weight of CP = 70.1 g/mol

Purity of CP = 95%

**Step 1:** To find pressure reduced ( $P_r$ ) and temperature reduced ( $T_r$ )

Data: Experimental number 16

At time 0, Pressure (P) = 7987.65 kPa = 78.83 atm

Temperature (K) = 276.85 K

At time  $t$ , Pressure (P) = 7238.00 kPa = 71.43 atm

Temperature (K) = 276.85K

Solution;

$$T_r = \frac{T}{T_c} = \frac{276.85 \text{ K}}{190.45 \text{ K}} = 1.45$$

$$\text{At time 0, } P_r = \frac{P}{P_c} = \frac{7987.65 \text{ kPa}}{4596 \text{ kPa}} = 1.74$$

$$\text{At time } t, \quad P_r = \frac{P}{P_c} = \frac{7238.00 \text{ kPa}}{4596 \text{ kPa}} = 1.57$$

**Step 2:** To find volume of gas phase ( $V_{cr}$ ), volume of additive ( $V_{add}$ ), and mole of water

Data: For 2.56% mol TBAB

Volume of reactor with reservoir ( $V_{reactor}$ ) = 146.94 cm<sup>3</sup>

Volume of Solution ( $V_{sol}$ ) = 30.00 cm<sup>3</sup>

Volume of gas phase =  $V_{reactor} - V_{sol} = 146.94 - 30.00 = 116.94 \text{ cm}^3$

Volume of additive ( $V_{add}$ )

For 2.56% mol of TBAB solution = 31.99% wt TBAB

$$= \frac{31.99 \text{ g TBAB}}{68.01 \text{ g H}_2\text{O}} \times \frac{1 \text{ g H}_2\text{O}}{1 \text{ ml H}_2\text{O}} \times \frac{1 \text{ ml TBAB}}{1.039 \text{ g TBAB}} \times 21 \text{ ml H}_2\text{O} \times \frac{100}{98}$$

= 9.7 ml in 21 ml H<sub>2</sub>O

So, in sol<sup>n</sup> 30.7 ml have TBAB = 9.7 ml

$$\text{In sol}^n \text{ 30.0 ml have TBAB} = \frac{9.7 \times 30.0}{30.7} = 9.48 \text{ ml}$$

$$\text{Volume of water} = V_{\text{sol}} - V_{\text{add}} = 30 - 9.48 = 20.52 \text{ ml}$$

$$\text{Mole of water} = 20.52 \text{ ml} \times \frac{1 \text{ mol}}{18 \text{ ml}} = 1.14 \text{ mol}$$

**Data: For 10%v/v CP**

= 10 ml in 90 ml H<sub>2</sub>O

So, in sol<sup>n</sup> 100 ml have CP = 10 ml

$$\text{In sol}^n \text{ 30.0 ml have TBAB} = \frac{10 \times 30.0}{100} = 3 \text{ ml}$$

$$\text{Volume of water} = V_{\text{sol}} - V_{\text{add}} = 30 - 3 = 27 \text{ ml}$$

$$\text{Mole of water} = 27 \text{ ml} \times \frac{1 \text{ mol}}{18 \text{ ml}} = 1.5 \text{ mol}$$

**Step 3:** To find compressibility factor (z)

$$\beta^0 = \frac{0.083 - 0.422}{T_r^{1.6}} = \frac{0.083 - 0.422}{1.45^{1.6}} = -0.15$$

$$\beta^1 = \frac{0.139 - 0.172}{T_r^{4.2}} = \frac{0.139 - 0.172}{1.45^{4.2}} = -0.10$$

$$\text{Time } 0; Z = 1 + \beta^0 \frac{P_r}{T_r} + \omega \beta^1 \frac{P_r}{T_r} = 1 + (-0.15) \left( \frac{1.74}{1.45} \right) + (0.0115) (-0.10) \left( \frac{1.74}{1.45} \right) = 0.8148$$

$$\text{Time } t; Z = 1 + \beta^0 \frac{P_r}{T_r} + \omega \beta^1 \frac{P_r}{T_r} = 1 + (-0.15) \left( \frac{1.57}{1.45} \right) + (0.0115) (-0.10) \left( \frac{1.57}{1.45} \right) = 0.8399$$

**Step 4:** To find the methane consumption : Data: Experimental number 16

$$\begin{aligned} \Delta n_{H_2} &= n_{H_2,0} - n_{H_2,t} = \left( \frac{PV}{zRT} \right)_{G,0} - \left( \frac{PV}{zRT} \right)_{G,t} \\ &= \left( \frac{78.83 \text{ atm} \times 116.94 \text{ cm}^3}{0.8148 \times 82.06 \text{ cm}^3 \cdot \text{atm/mol} \cdot \text{K} \times 276.85 \text{ K}} \right)_{G,0} \\ &\quad - \left( \frac{71.43 \text{ atm} \times 116.94 \text{ cm}^3}{0.8399 \times 82.06 \text{ cm}^3 \cdot \text{atm/mol} \cdot \text{K} \times 276.85 \text{ K}} \right)_{G,t} \end{aligned}$$

$$= 0.4929 - 0.4378 = 0.0551$$

So, the methane consumption = 0.0231 mol

$$\text{Gas uptake} = \frac{0.0551 \text{ mol}}{1.50 \text{ mol of H}_2\text{O}} = 0.03672 \text{ mol/mol of H}_2\text{O}$$

The calculation for the methane released has similar step with the methane consumption, but the equation is calculated by

$$\Delta n_{H,t} = n_{H,t} - n_{H,0} = \left( \frac{PV}{zRT} \right)_{G,t} - \left( \frac{PV}{zRT} \right)_{G,0}$$

Where  $\Delta n_{H,t}$  = moles of released gas from the hydrate

$n_{H,t}$  = moles of hydrate at time  $t$ , mol

$n_{H,0}$  = moles of hydrate at time 0, mol

$P$  = pressure of the crystallizer, atm

$T$  = temperature of the crystallizer, K

$V$  = the volume of gas phase in the crystallizer,  $\text{cm}^3$

$z$  = compressibility factor

$R$  =  $82.06 \text{ cm}^3 \cdot \text{atm} / \text{mol} \cdot \text{K}$

## Appendix B Calculation for the Methane Hydrate Yield

From;

$$\text{Methane hydrate yield (mol\%)} = \frac{\text{Methane consumed (mol)}}{\text{Methane input (mol)}} \times 100$$

Methane consumed = 0.0551 mol

Methane input = 0.4929 mol



Thus,

$$\text{Methane hydrate yield (mol\%)} = \frac{0.0551 \text{ mol}}{0.4929 \text{ mol}} \times 100 = 11.17 \text{ mol\%}$$

### Appendix C Calculation for the Percentage of Methane Recovery

From;

$$\% \text{Methane recovery} = \frac{(\Delta n_{H_2})_t}{(\Delta n_{H_2})_{t_{\text{end}}}} \times 100$$

where  $(\Delta n_{H_2})_t$  = moles of released gas from the hydrate during the hydrate dissociation at any given time

$(\Delta n_{H_2})_{t_{\text{end}}}$  = moles of gas consumption for hydrate formation at the end of experiment

Data:  $(\Delta n_{H_2})_t$  = 0.0074 mol

$(\Delta n_{H_2})_{t_{\text{end}}}$  = 0.0367 mol

Thus,  $\% \text{Methane recovery} = \frac{0.0074}{0.0367} \times 100 = 20.02\%$

## CURRICULUM VITAE

**Name:** Ms. Chutikan Jaikwang

**Date of Birth:** November 30, 1990

**Nationality:** Thai

**University Education:**

2010–2014 Bachelor Degree of Science (B. Sc. Industrial Chemistry) (First Class Honours), Faculty of Applied Science, King Mongkut's University of Technology North Bangkok, Bangkok, Thailand

**Work Experience:**

2012-2013 Position: Internship Student (Quality Assurance)  
Company name: J R M. CO., LTD

**Proceedings:**

Jaikwang, C., Rangsunvigit, P., and Kulprathipanja, S. (2017 May 23) Assisted Methane Hydrate Formation with the Addition of Promoters. Proceedings of The 8<sup>th</sup> Research Symposium on Petroleum, Petrochemicals and Advanced Materials and The 23<sup>th</sup> PPC Symposium on Petroleum, Petrochemicals, and Polymers, Bangkok, Thailand.

**Presentations:**

Jaikwang, C., Rangsunvigit, P., Kulprathipanja, S. (2017, June 12-15) Methane hydrate formation and dissociation in the presence of different cyclopentane (CP) and tetra-n-butyl ammonium bromide (TBAB) solution. Poster presented at 2<sup>nd</sup> International Conference on Applied Surface Science, Dalian, China.